



OPEN ACCESS

EDITED BY

Daniele Spatola,
Sapienza University of Rome, Italy

REVIEWED BY

Eleonora Martorelli,
National Research Council (CNR), Italy
Attilio Sulli,
University of Palermo, Italy

*CORRESPONDENCE

Agostino Meo,
✉ a.meo@unisannio.it

RECEIVED 17 February 2023

ACCEPTED 15 May 2023

PUBLISHED 31 May 2023

CITATION

Meo A and Senatore MR (2023),
Morphological and seismostratigraphic
evidence of Quaternary mass transport
deposits in the North Ionian Sea: the
Taranto landslide complex (TLC).
Front. Earth Sci. 11:1168373.
doi: 10.3389/feart.2023.1168373

COPYRIGHT

© 2023 Meo and Senatore. This is an
open-access article distributed under the
terms of the [Creative Commons
Attribution License \(CC BY\)](https://creativecommons.org/licenses/by/4.0/). The use,
distribution or reproduction in other
forums is permitted, provided the original
author(s) and the copyright owner(s) are
credited and that the original publication
in this journal is cited, in accordance with
accepted academic practice. No use,
distribution or reproduction is permitted
which does not comply with these terms.

Morphological and seismostratigraphic evidence of Quaternary mass transport deposits in the North Ionian Sea: the Taranto landslide complex (TLC)

Agostino Meo* and Maria Rosaria Senatore

Department of Science and Technology, University of Sannio, Benevento, Italy

The Taranto Landslide Complex (TLC) is a large submarine landslide area located along the continental margin of the Puglia Region, in the Gulf of Taranto (North Ionian Sea), between 200 and 800 m water depth. Based on very high-resolution multibeam data, a morphological analysis was performed by measuring different physical and spatial parameters (i.e., surface, headwall height and length, slope in the source area, and blocks in the accumulation zone). In addition, we use nine high-resolution sub-bottom CHIRP profiles to reconstruct the stratigraphic architecture. The main results show five phases of Quaternary mass transport deposits (MTDs) in the study area. The oldest to the youngest are MTD1, with a volume of about 0.032 km³ and an area of about 4 km²; MTD2, which is the largest of the identified deposits, covering an area of ~26 km² and having an estimated volume of ~0.35 km³; and MTD3 and MTD4, with volumes of about 0.033 km³ and 0.035 km³ and an area of 7 km² and 5 km², respectively. The final submarine landslide is represented by MTD5, which has a volume of 0.02 km³. The deposits are internally characterized by chaotic acoustic facies with reflectors with moderate amplitude and laterally continuous in time, showing likely erosive characteristics defined as “bounding surfaces”. The main transport direction of the MTDs is from north/northeast to south/southwest. This represents the trend of the continental slope, but there is also slope failure evidence coming from west/northwest to east/southeast (MTD5). The correlation between topographic and seismo-stratigraphic features allows the documentation of the characteristics, distributions, sources, and the triggering mechanisms of the Late Quaternary MTDs in the area. We suggest that still the unknown trigger mechanisms could be based on the performed analysis, related to the anomalously high sedimentation rates and/or sea level fluctuation.

KEYWORDS

mass transport deposits, submarine landslide complex, Ionian sea, high-resolution multibeam data, seismic characteristics

1 Introduction

Submarine landslides have occurred in several geological contexts worldwide, covering a wide range of geological settings from passive to active continental margins, rivers, pro-deltas and submarine fans, on volcanic islands, and glaciated and sediment-starved margins (Hampton et al., 1996; Hühnerbach et al., 2004; Masson et al., 2006; Twichell et al., 2009; Huhn et al., 2019). Submarine landslides are a coherent translational movement along a planar glide surface without internal deformation (Mulder and Cochonat, 1996; Moscardelli and Wood, 2008). During sediment destabilization, a slide may evolve into a coherent rotational movement (Huhn et al., 2019). When it is not possible to define a single slide, we speak of composite events (mass transport complexes). These have been increasingly recognized along different continental margins through enhanced resolution bathymetric maps (Lastras et al., 2002; 2004; Gamberi et al., 2011; Rovere et al., 2014) and 2D/3D seismic reflection data (Moscardelli et al., 2006; Dalla Valle et al., 2013) and by combining diverse data sets across different scales and resolutions (Georgiopoulou et al., 2018). Mass transport complexes are the result of the emplacement of sedimentary bodies with a high variety of internal geometries (translated or thrust blocks and chaotic facies), which are termed “mass transport deposits” (MTDs).

MTDs are sedimentary bodies formed by sediment instability in marine environments (McAdoo et al., 2000a; Moscardelli et al., 2006; Bull et al., 2009; Alves, 2015). They are important not only because of their volumetric significance in the sedimentary record (Gamboa et al., 2010) but also because they reshape the seafloor morphology and continental margins (Gee et al., 2007; Alves, 2010; Strasser et al., 2011; Gamboa and Alves, 2015). Submarine geohazards are often linked with MTDs (Tappin et al., 2001; Locat and Lee, 2002; Masson et al., 2006; Lee, 2009; Chiocci and Ridente, 2011; Talling et al., 2013; 2014; Alves, 2015; Casalbore et al., 2020a; Sulli et al., 2021a). The genesis of MTDs can be influenced by a number of factors, such as sea level change (Smith et al., 2013; Urlaub et al., 2013), high sedimentation rates (Locat and Lee, 2002; Dalla Valle et al., 2013), earthquakes (Davies and Clark, 2006; Moscardelli et al., 2006; Kawamura et al., 2014), slope gradient (Canals et al., 2004; Owen et al., 2007), tectonic and volcanic activities (Lamarche et al., 2008; Masson et al., 2008; Alves, 2015; Casalbore et al., 2020b; Sulli et al., 2021b), and free gas accumulation (Hühnerbach and Masson, 2004; Sultan et al., 2004; Maslin et al., 2005; Talling et al., 2014; Horozal et al., 2017; Gross et al., 2018). Another precondition factor for mass-wasting processes can be the role of fluid seepage on the seabed (Skarke et al., 2014; Spatola et al., 2018a; Spatola et al., 2018b; Micallef et al., 2019; Spatola et al., 2020).

In this study, we used very high-resolution morphobathymetric data and sub-bottom profiles to analyse the Taranto landslide complex (TLC) on the continental slope of the Gulf of Taranto in the North Ionian Sea. This area has been interpreted as a single mass transport event (Meo et al., 2018a; Senatore et al., 2022), but new results show the presence of five different MTDs. We studied seafloor morphology, internal geometry, and stacking architecture, and identified specific echo facies of the mass transport complexes. We present interpretation of triggering mechanisms for the failure events and propose an evolutionary model for the TLC.

2 Geological setting

The Gulf of Taranto is the northern tip of the Ionian Sea (Figure 1A), bordered by the Calabria, Basilicata, and Puglia regions. It is located between an orogenic belt (southern Apennine Chain and Calabrian Arc) and the Apulia foreland. It represents an area of foredeep (Figure 1A) in a mature stage since the front of the thrust sheets is close to the Apulia foreland (Senatore, 1988).

The southern Apennine chain is composed of units derived from the subduction of neo-Tethys oceanic lithosphere beneath the European plate (Cosentino et al., 2010; Carminati et al., 2012; Vitale & Ciarcia, 2013; Vitale et al., 2019). During the Mesozoic, this margin was characterized by a prevalently tensile tectonic regime, and the sedimentary domains were represented by a succession of carbonate neritic platforms and deep basins (D'Argenio et al., 1973; Carannante et al., 1997; Catalano et al., 2001; Mazzoli et al., 2001; Iannace et al., 2011; Vitale and Ciarcia, 2022). Some authors hypothesise transcurrent movements as a major structural control (Horvarth and D'Argenio, 1985). Tectogenesis shifted eastwards and southwards in the Neogene and Quaternary (Catalano et al., 2004); the Southern Apennines have consequently assumed their present configuration, with the Gulf of Taranto as the foredeep, located between the allochthonous thrust sheets of the chain to the west and the Apulia foreland to the east (Pescatore and Senatore, 1986; Senatore et al., 1988; Finetti, 2003; Senatore et al., 2021a; Senatore et al., 2021b).

The eastern units of the Gulf of Taranto lie over the Apulia carbonate succession (Mostardini & Merlini, 1986; Patacca & Scandone, 1989), which represents part of the Adriatic foreland of the Apennine chain mainly affected by tensile movements. During the Quaternary, Apulia was still affected by mild brittle deformation with rare faults and characterized by small offset (Di Bucci et al., 2011; Mastronuzzi et al., 2011). Distinctive tectonic behaviours have been recognised on the basis of extensive outcrops of marine deposits ascribed to Marine Isotopic Stage MIS5. Since the Middle Pleistocene, the Ionian coast from Taranto to Gallipoli was characterized by uplift values from 0.31 mm/year to 1.21 mm/year (Bordoni and Valensise, 1999; Ferranti et al., 2006). Several authors have determined that the rate of uplift of this area since the Middle Quaternary was an uplift-rate of 1.7–1.8 to 0.4 mm/year from SW to NE (Caputo and Bianca, 2005; Caputo et al., 2010; Teofilo et al., 2018) and have hypothesised that, along the coastal sector of the Gulf of Taranto, a compressive regime is still active (Figure 1A).

3 Materials and methods

The dataset used to study the TLC is composed of multibeam (MBES) data and sub-bottom CHIRP profiles collected during two research expeditions (CONISMA 11/10 and SAND) on the R/V *Minerva Uno*.

The multibeam data were acquired using a 50-kHz Reason Seabat 8160 MBES system for a total of 670 nautical miles from the outer shelf at a depth of 150 m down to the base of the Apulian continental slope at a depth of 1,000 m. The MBES data were processed using Caris HIPS™ and SIPS™ software applications, corrected for the tidal variations and merged to produce a DEM (digital elevation model) of

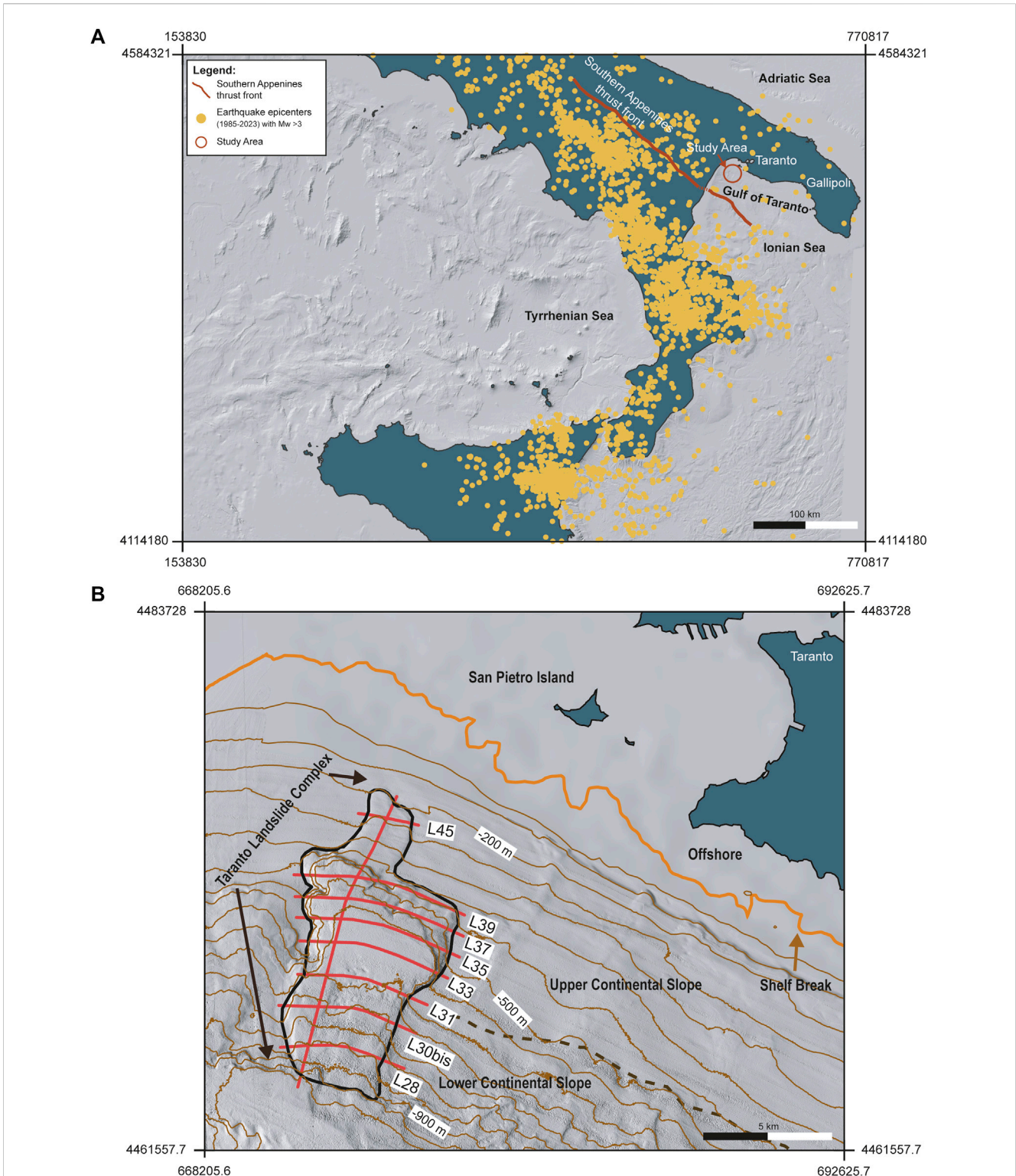


FIGURE 1

(A) Location of the study area with high-resolution multibeam data along the Gulf of Taranto (North Ionian Sea) with allochthonous thrust front of the Southern Apennines (red line). Yellow points show earthquake epicenters (1985–2023) with Mw >3 (from [ISiDe working Group, 2016](#) (Italian Seismological and instrumental Data-BasE) and European-Mediterranean Seismological Centre CSEM-EMSC, 2013 Catalogue). (B) Shaded relief of the sector impacted by the Taranto Landslide Complex (TLC). Red lines represent the location of the sub-bottom CHIRP profiles; orange line is the shelf break brow; dashed line represents the morphologically divided the upper continental slope (UCS) and lower continental slope (LCL). Contours are also shown (brown lines)—contour interval is 50 m.

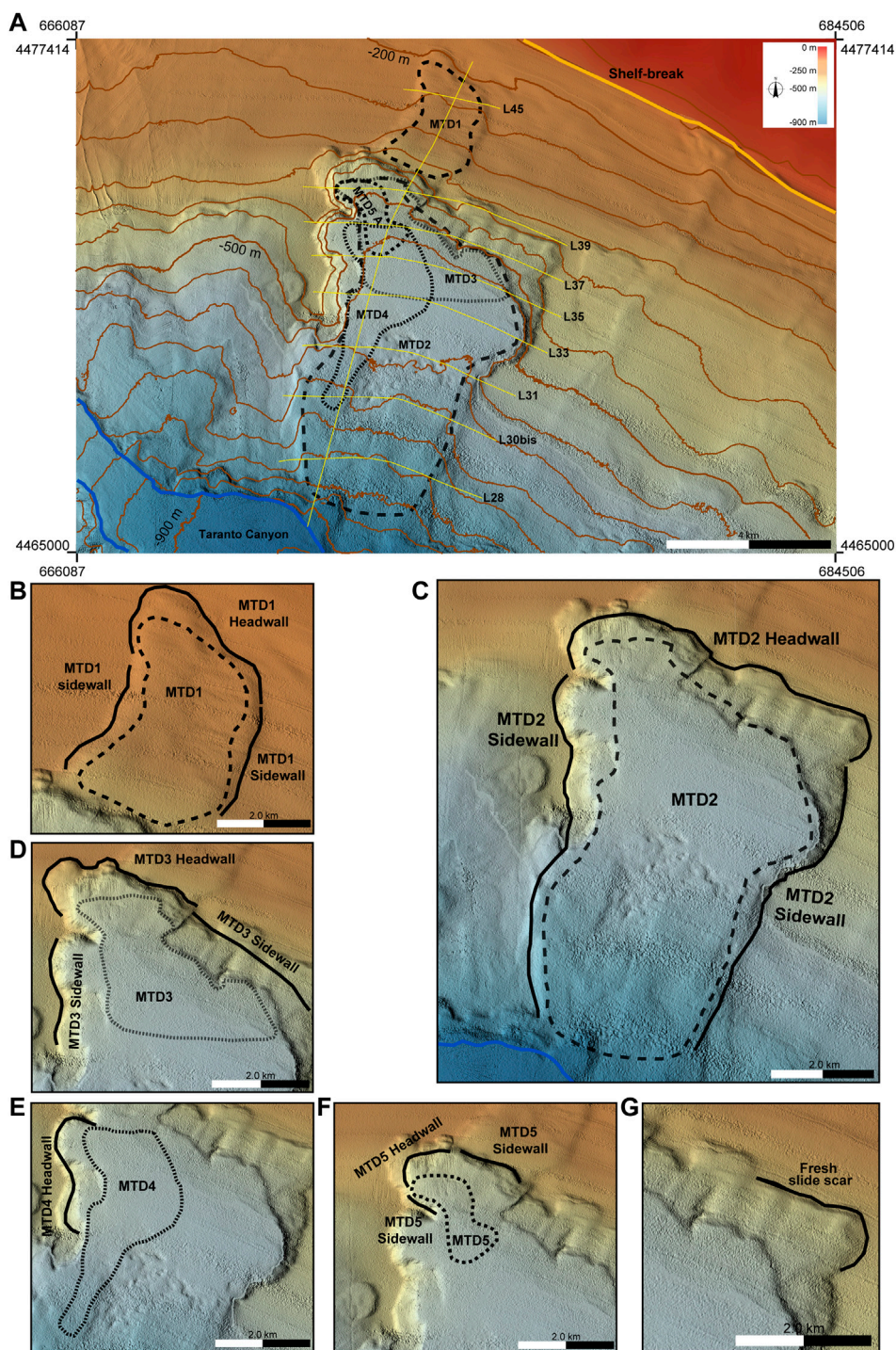


FIGURE 2

(A) Multibeam bathymetry maps showing the location of the TLC with the areal extension of its building MTDs (MTD1, MTD2, MTD3, MTD4, and MTD5). Location of the sub-bottom CHIRP profiles is reported. (B–F) The morphological features (Headwall and Sidewall) for each MTD and the limit of the deposit are shown. (G) Secondary slide scar along the MTD2 headwall characterized by a rough surface texture defined as “fresh slide scar”. Contour interval is 50 m.

the seafloor. We gridded the bathymetric data with Global Mapper software (<https://www.blumarblegeo.com/global-mapper/>) to create a bathymetric map with a spatial resolution of 20 m.

The dataset includes nine sub-bottom CHIRP profiles (on the slope 8 strike and 1 dip oriented—Figure 1B) acquired with a hull-mounted 16-transducer GeoAcoustic GeoChirp II at 0.5–13 kHz

TABLE 1 MTD unit and morphometric parameters of the Taranto Landslide Complex.

MTD unit	Headwall mean water depth (m)	Headwall length (km)	Maximum headwall height (m)	Fall height (H)	Evacuation area (Km ²)	Runout (R) (m)
MTD1	200	1.8	30	180	1	2,500
MTD2	410	5.9	95	465	1.5	7,300
MTD3	360	2.6	95	275	0.9	3,350
MTD4	450	2.3	85	255	0.8	4,600
MTD5	350	1.1	60	230	0.2	2000

with decimeter-scale resolution. Kingdom suite software was used to interpret the seismic profiles.

Estimating the volume of sediment accumulated in the downslope depositional section involved defining an MTD's areal extension and the mean thickness of deposits. An average P-wave velocity of 1,600 ms⁻¹ was used to define the thickness of the slide deposits (Omeru and Cartwright, 2015).

Finally, in order to reconstruct the phases of the MTD emplacement, we developed an implementation model based on the analysis of high-resolution morphobathymetric data and of sub-bottom CHIRP profiles, and spatial and temporal relationships between each MTD.

4 Results

4.1 General morphology of the area

The study area is located on the Apulia continental slope, which starts at the shelf break at about 120 m depth. The continental slope can be divided into the upper continental slope (UCS) and lower continental slope (LCS). The UCS develops between 120 m and 450 m water depth with an average slope gradient of 3°. In this sector, the seafloor has a smooth topography and is locally characterized by a few morphological features. The LCS extends between 450 m and 900 m water depth with an average slope gradient of 4°–5°. The main morphological feature of this part of the slope is represented by widespread slope instability features (Figure 1B).

4.2 Morphology of the Taranto Landslide Complex (TLC)

The TLC is a complex along the slope of the northern part of the Gulf of Taranto located at 200–800 m water depth (Figure 1B). It is the most northern landslide area of the Gulf of Taranto and is also one of the largest (in terms of extension) submarine mass movements identified along the Apulian continental slope. Through the integration of high-resolution multibeam data and sub-bottom CHIRP profiles, we identified five buried MTDs: MTD 1–5 (Figure 2A).

4.2.1 MTD1

MTD1 is the oldest mass transport deposit, located in the northern part of the TLC and affects the continental slope about

0.6 km from the shelf-edge (Figures 2A, B). It is sub-circular in shape; it has a length from headwall to the lower part of about 2 km and a width of 1–2 km. The headwall has a length of about 2 km, a height of up to 30 m (Table 1), and an area of about 4 km² (Table 2). The high resolution bathymetric and seismic profiles datasets show that MTD1 is truncated by the headwall of MTD2, the second oldest landslide in the complex (Figure 2A).

4.2.2 MTD2

MTD2 is the largest mass transport deposit of the area and develops from 400 to 800 m water depth from the toe of MTD1 down to the base of the slope, covering an area of about 26 km² (Figures 2A, C; Table 2). The headwall has a NW–SE trend, a length of about 6 km, and an area of 1.5 km² (Table 1). The slope gradient is about 8° with a maximum height of 95 m. The headwall surface is furrowed by gullies, which extend perpendicularly with an average length of about 600 m. The accumulation zone of MTD2 begins at a depth of 570 m, where a rough morphology is present due to blocks 100 m–150 m long and 10–20 m high (Figure 2C) on the seafloor. MTD2 covers a length of 7.3 km and a width of 3.7 km. The toe domain, which represents the terminal part of the displaced sediments, is located between 770 m and 800 m water depth; it is possible to observe that the sediments involved in the landslide have undergone intense erosive processes due to currents flowing inside the Taranto Canyon (Figure 2A).

The left sidewall, developed from about 550 m to 900 m water depth, shows good spatial continuity extending for a length of about 6 km with a slope gradient of about 4°. The right sidewall is affected by the evidence of several scars linked to minor mass movement that has reshaped the morphology by forming a ridge extending approximately 10 km with slopes ranging from 10° to 20° from a depth of about 400 m–750 m.

4.2.3 MTD3

MTD3, which is NNW–SSE trending, covers an area of about 7 km² (Table 2). Its source area is located within the MTD2 headwall area (Figure 2A). In the upper part, MTD3 has a width of about 1.7 km, enlarging progressively downslope and reaching about 3.5 km in its terminus (Figure 2D). The headwall of MTD3 is about 2.5 km long with an area of about 1 km² and a maximum height of 95 m (Table 1). The northern MTD3 sidewall is a part of the MTD2 headwall, while the southern sidewall corresponds to the headwall of MTD4 (Figure 2D). The accumulation area is found at a depth of 570 m, and its runout distance is about 3.3 km (Table 1).

TABLE 2 MTD units with relative time of occurrence, source direction, areal extent and thickness, and volume of each corresponding unit.

MTD unit	Relative time of occurrence	Source direction	Area extent (km ²)	Min. thick. (m)	Max. thick. (m)	Mean thick. (m)	Volume (km ³)
MTD1	1	N	4	2	11	8	0.032
MTD2	2	N	26	6	36	14	0.35
MTD3	3	NNW	7	6	16	4	0.033
MTD4	4	W	5	5	17	6	0.030
MTD5	5	NNW	5	4	14	4	0.02

4.2.4 MTD4

MTD4 is located in the western sector of the TLC at a depth of 540 m. The MTD4 headwall is up to 2.3 km long, between 80 and 85 m high, and is carved into the MTD2 sidewall (Figures 2A, E). MTD4 covers an area of 5 km² (Table 2), extending down to 670 m with a total runout distance of about 4.5 km (Table 1). It is impossible to identify the developed sidewalls of MTD4. Moreover, the presence of the oldest MTDs (MTD2 and MTD3) influences the shape of MTD4.

4.2.5 MTD5

MTD5 covers an area of about 5 km² (Table 2) and is the smallest and the youngest deposit. The MTD5 headwall has a length of about 1 km and height of about 60 m (Table 1) and corresponds to a part of the MTD3 headwall (Figures 2A, F). The sidewalls are represented by the headwalls of MTD2 (northern sidewall) and MTD4 (southern sidewall), respectively. The measured runout is about 2.0 km.

A secondary slide scar crossing the eastern side of the MTD2 headwall has been observed (Figure 2G). This scar has a relief of 95–120 m, a length of about 1.5 km, and extends along the slope up to ~500 m depth. This scar, characterized by a rough surface texture and lacking a substantial sediment drape, could be a relatively “fresh feature.” Although the multibeam data clearly show this scarp, it was not possible to identify, in the sub-bottom CHIRP profiles, the related MTD.

4.3 MTD seismic facies

The sub-bottom CHIRP profiles (Figure 1) allow identification of the seismic facies of the mass-wasting events. The five mass transport deposits mapped in the area are characterized by facies from chaotic with intermittent, indistinct discontinuous reflectors, at times with regular small hyperbolae. Furthermore, each MTD is separated by reflectors with moderate to low amplitude and continuity (Bull et al., 2009; Cheng et al., 2021). These reflectors are defined as bounding surfaces (BSs), all of which have erosive characteristics. In order to define the stratigraphic framework for each mass transport event and to reconstruct the evolution of the TLC, five BSs (1–5 from oldest to youngest) were tracked (Figures 3–9). The main seismic characteristics of each MTD are shown in Table 3.

MTD1 is identified by the presence, at the base, of the reflector BS1. Its maximum thickness is 13.7 ms reached in correspondence

with both the TSV1 and L45 crossing profiles (Figures 3C, 4). MTD1 is almost entirely characterized by seismic facies from chaotic sub-bottom to intermittent, indistinct, discontinuous sub-bottom with regular small hyperbolae. The estimated volume of the sediments involved in the movement is about 0.032 km³. To the south, MTD1 is truncated by the presence of MTD2, which is the second oldest and biggest MTD of the complex. It is bounded by BS2, which corresponds to the basal shear surface of MTD2 and is characterized by seismic facies from chaotic sub-bottom to intermittent, indistinct, discontinuous sub-bottom. The maximum thickness of MTD2 is about 45 ms. Its depocenter is elongated in a N–S direction and is located in the central TLC along the profile L31 (Figures 8A, B); in the seismic profile downslope of the headwall area (along the profile L31 and L30bis), several blocks were imaged (Figure 8). These show a hummocky seafloor and no sub-bottom reflectors, indicating that they are associated with landslides. Towards the toe, above MTD2, several acoustic anomalies are shown (Figure 9). The volume of MTD2 is about 0.35 km³.

BS3 marks the base of MTD3, which is shown from chaotic to intermittent seismic reflectors and indistinct background, discontinuous with some small hyperbole. It has a NW–SE flow direction with a runout of about 3.5 km; its depocenter is identified at the intersection between profiles L39 and Tsv1 (Figures 3D, 5A, B), with a thickness of about 20 ms. MTD3 covers MTD2 up to 580 m water depth along an area of about 7 km² and has an estimated volume of about 0.033 km³.

MTD4, showing from chaotic to intermittent, indistinct, discontinuous sub-bottom seismic reflectors with some small hyperbolae, is located along the sidewall of MTD2; its source area is WNW–ESE (Figures 3D, 5C, D; 6, 7; 8A, B). The estimated volume of sediment involved is 0.035 km³, and it covers an area of about 5 km² with a runout of 4.5 km and an almost N–S trend. The related bounding surface is BS4, and the maximum thickness is 21 ms (in the WNW part of the L37 profile—Figures 5C, D) that represents the depocenter of the deposit. MTD4 has mantled the underlying MTD2, and, in correspondence of the blocks, the onlap geometry of the reflections is present (Figures 8A, B).

MTD5 shows seismic facies from chaotic sub-bottom to intermittent, indistinct, discontinuous sub-bottom. Its areal extent is very limited, and it is bounded by another erosional surface (BS5) on both MTD3 to the north and on MTD4 to the south. Therefore, between MTD5 and MTD3 (to the north) and between MTD5 and MTD4 (to the south), a thickness of sediments with regular and continuous reflectors is present. The latter is thicker to the north, about 17.5 ms, while, to the south, it reaches about 12.5 ms

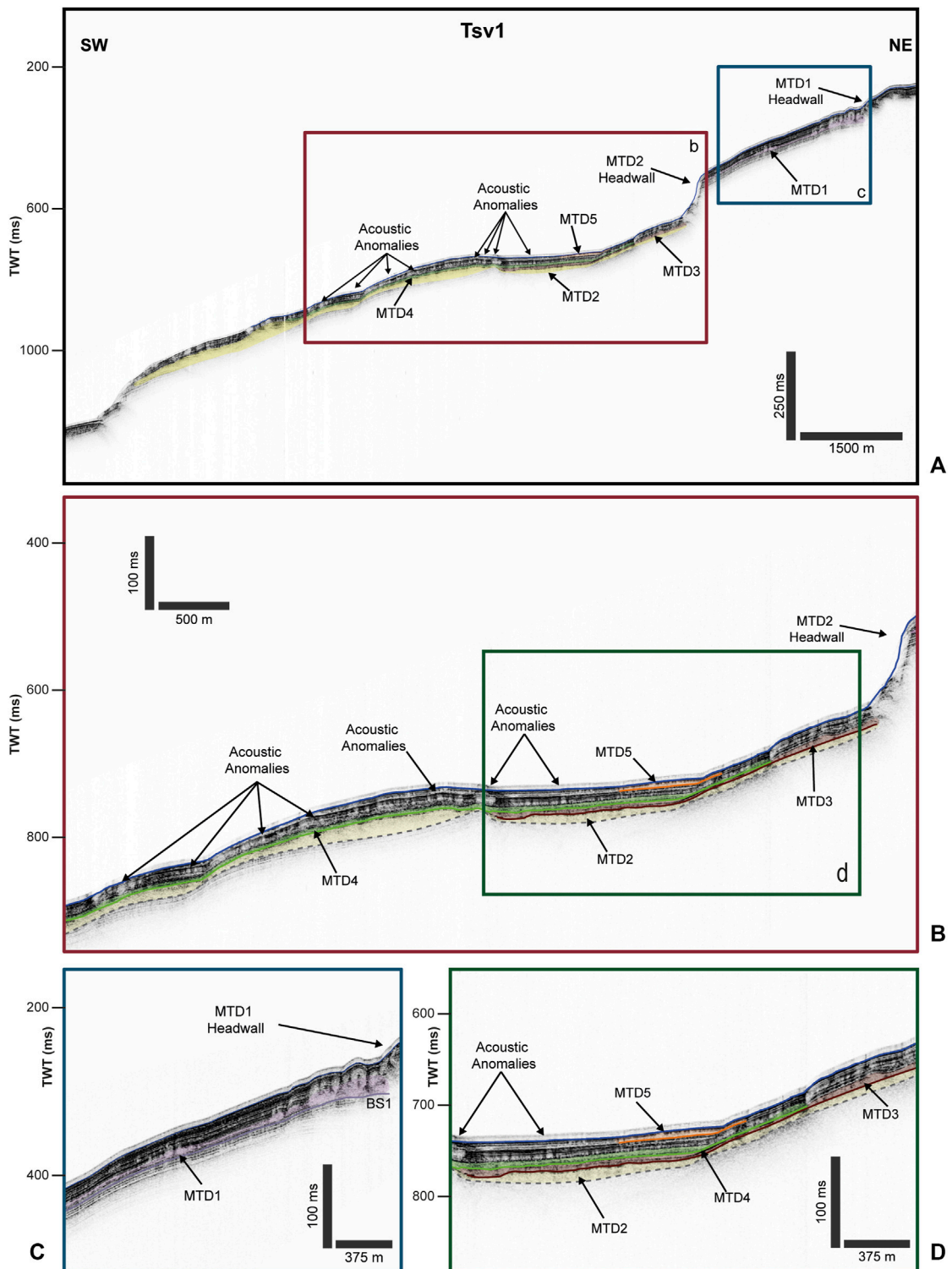


FIGURE 3

(A) CHIRP seismic profile Tsv1, illustrating the stratigraphic framework of the TLC and the relations between MTDs. The brown and blue boxes represent the zoom shown in (B,C). (B) CHIRP profile illustrating internal geometries and spatial relationships between MTDs (see Figure 1B for the location of the profiles); the green box is the blow-up reported in (D). (D) Blow-up showing the seismic characteristics and relationship between MTDs identified in the TLC. The morphological features are also indicated (see Figure 1B for the location of the profile).

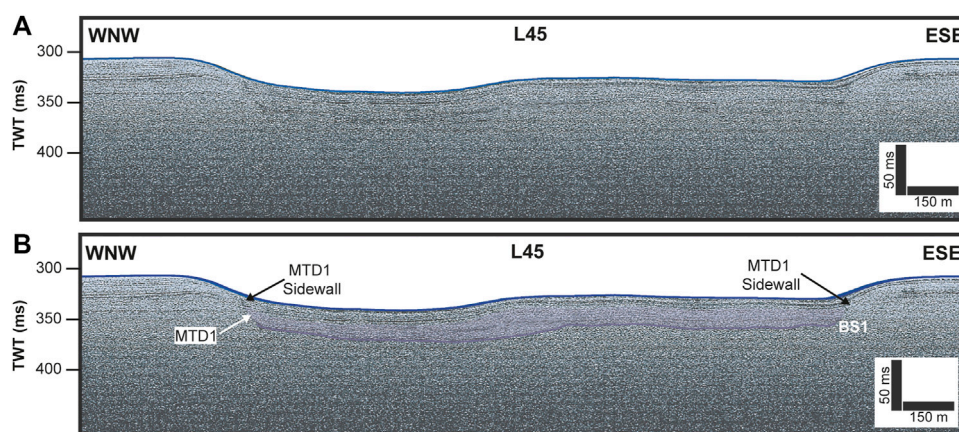


FIGURE 4

(A) Uninterpreted and (B) interpreted images of the CHIRP profile L45. The interpreted section shows the position of the MTD1 in the sub-bottom and the location of the sidewalls. The morphological features are also indicated (see Figure 1B for the location of the profile).

(Figures 3D, 5). The source area is NW–SE, the runout is about 2 km, the thickness is 17.5 ms, and the estimated volume involved is about 0.02 km³.

5 Discussion

5.1 MTD source direction, volume, and age

The proposed distributions and flow directions of the MTDs in the study area are shown in Figure 10. Their source areas are mainly from the north and north–northwest sectors of the continental slope, except the MTD4 source area, which comes from the west. The main trend probably depends on predisposing factors (continental slope trend) and/or triggering factors. The approach to calculate the volume of sediment accumulated in the downslope depositional section involved the attribution to the slide deposit at an appropriate P-wave velocity. We used an average seismic velocity of 1,600 ms⁻¹ (Omeru and Cartwright, 2015).

The estimated volumes of the investigated MTDs are between 0.02 and 0.35 km³ (Table 2). The biggest MTD (in terms of estimated volume) of the TLC is represented by MTD2, which has a volume of about 0.35 km³—very similar to the landslides of the catalogue of the Mediterranean Sea (Urgeles and Camerlenghi, 2013). Regarding the age of the deposits, we tried to make a correlation with the sedimentation rate measured in the Gulf of Taranto by Grauel (2012). We propose a sedimentation rate in this area of 70 cm/ky. Therefore, by analysing the CHIRP seismic profiles, we measured the thicknesses of the overlying post-mass-flow sediments between each MTD phase, particularly in profiles L35 and L33 (Figures 6, 7). The relation between the sedimentation rate and the thickness of the overlying post-mass-flow sediments allowed us to identify two moments of activation for MTDs. The first likely occurred about 25–26 ky BP when MTD1 and MTD2 were triggered. The second involved MTD3 and MTD4 and happened approximately 20–21 ky BP. Furthermore, we defined the thicknesses of the overlying post-mass-flow sediments between MTD4 and the seafloor. This

measure, carried out along the profile L33—where the post-mass-flow sediments are well-developed (Figure 6)—determined a thickness of about 13 m. Finally, MTD5 is observed; its location on the seafloor probably testifies to an actual mass-wasting process of the TLC (Figures 3D, 5).

5.2 Trigger mechanism

According to Shanmugan and Wang (2015), a triggering mechanism represents a primary process that causes changes in the physical, chemical, and geotechnical properties of soil, resulting in the loss of shear strength that initiates sediment failure and movement.

A triggering mechanism, or a combination of triggering mechanisms, is required to destabilize sediments already prone to failure. Excess pore pressure generation and the presence of mechanically weak layers, or a combination of both, are unequivocally recognized as key parameters influencing slope stability (Sultan et al., 2004; Huhn et al., 2019) and might explain the recurrence of events (Gatter et al., 2021). In the case of the TLC, the exact triggering mechanism is unknown, although we tentatively suggest that the landslide was probably started by the following combination of mechanisms.

5.2.1 High sedimentation rate

An anomalous high sedimentation rate could be one of the possible MTD triggering mechanisms, which can lay the sediment foundation for the formation of MTDs (Dugan and Flemings, 2000; Locat and Lee, 2002; Forsberg et al., 2007; Dugan and Sheahan, 2012; Talling et al., 2014; Yamamoto et al., 2019). The proposed model for the development of the TLC is based on Masson et al. (2008), which described the short-term accumulation of a large amount of sediments on the continental slope; sedimentation rates are highest on the upper slope, creating high pore pressures that lead to slope failure (Figure 11). The resulting landslides then propagate downslope through a combination of slope loading and the erosion

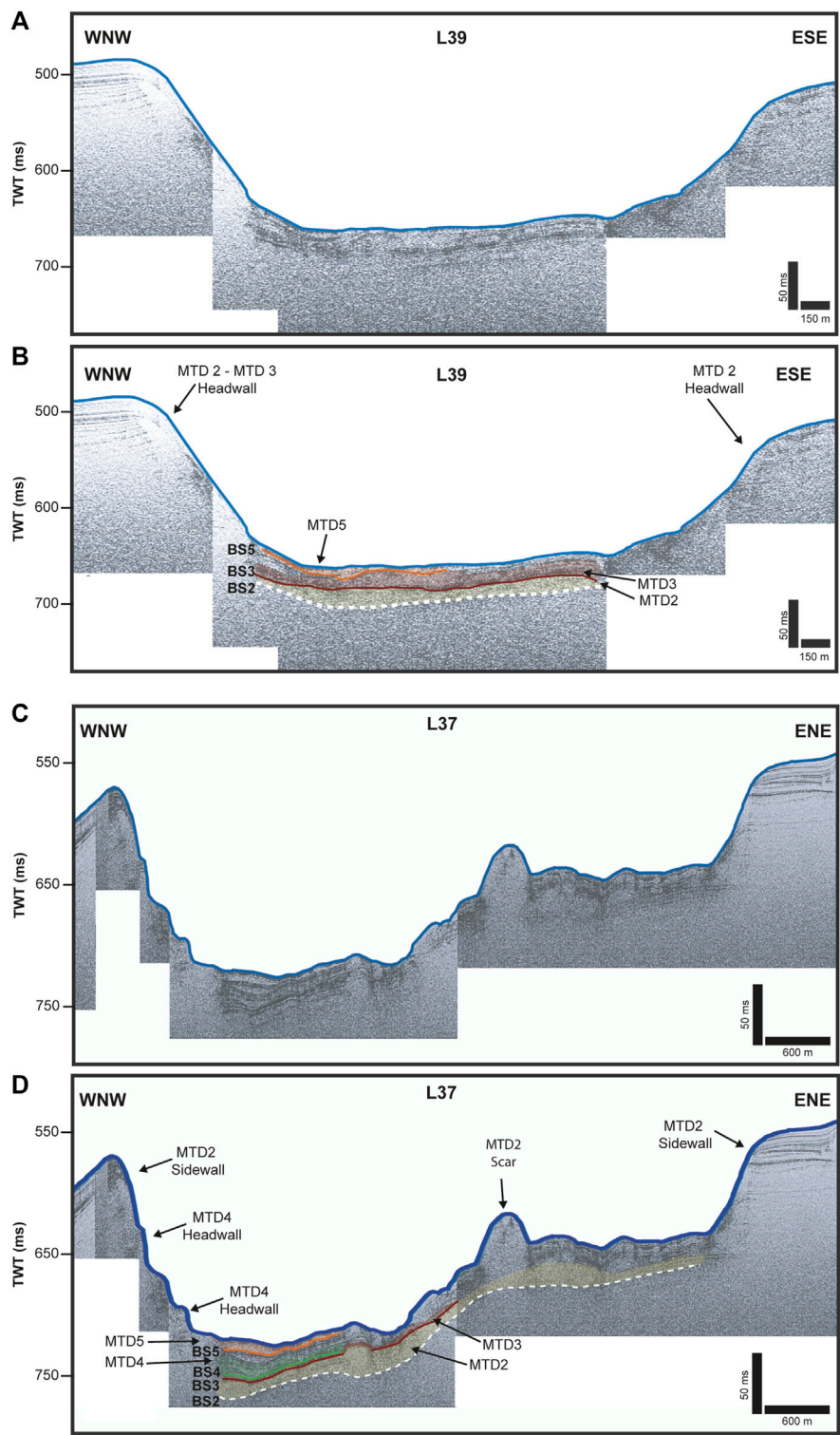


FIGURE 5
 (A) Uninterpreted and (B) interpreted images of the CHIRP profile L39. The interpreted section shows the relation between MTD2 and MTD3 separated by a bounding surface. (C) Uninterpreted and (D) interpreted image of the CHIRP profile L37, showing the position and relation between MTD2, MTD3, and MTD4. The morphological features are also indicated (see Figure 1B for the location of the profile).

of superficial slope sediments (Gee et al., 2007). Indeed, following Grauel et al. (2012) and Leynaud et al. (2009), we infer the age of MTD1 and MTD2 at about 25–26 ky BP, and 20–21 ky BP for

MTD3 and MTD4. It is probable that, during sea level fall and the last lowstand stage, a large mass of sediment settled on the continental shelf at the break and caused an increase of pore

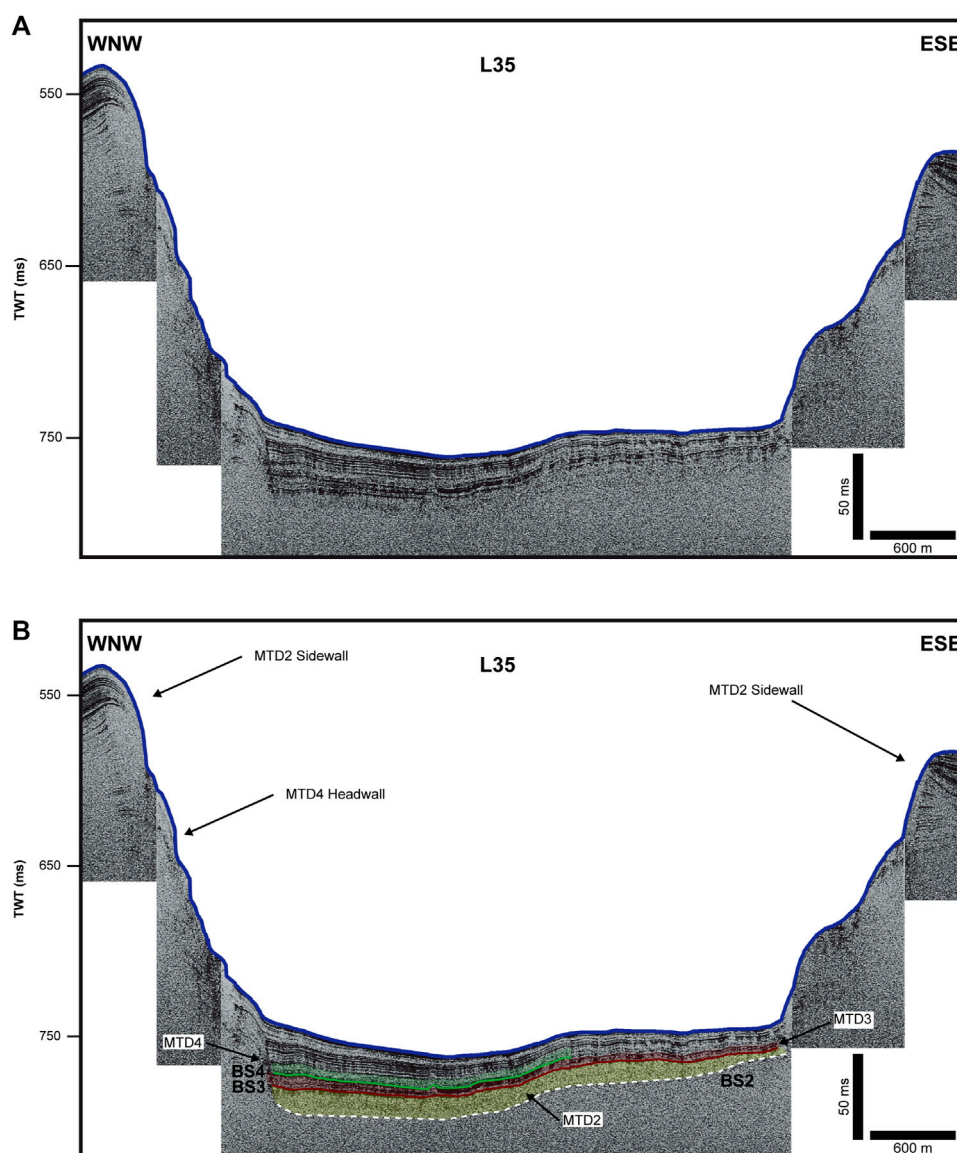


FIGURE 6

(A) Uninterpreted and (B) interpreted images of the CHIRP profile L35. The profiles show the bounding surfaces between MTD2, MTD3, and MTD4 and the relationships between them. The morphological features are also indicated (see Figure 1B for the location of the profile).

pressures within the sediments. Subsequently, the migration of pore fluids in overpressured formations caused the downslope area to be unstable and to collapse, thereby forming the MTDs.

5.2.2 Sea level change

The role of sea level change as a trigger for submarine landslides is still unclear. Smith et al. (2013). Talling et al. (2014) suggest hydrostatic pressure as a possible cause for submarine slope failure. In fact, rapid changes in sea level linked to sediments with very low permeability could generate transient interstitial overpressure (Smith et al., 2013). Urlaub et al. (2013), performed statistical analysis on 68 submarine landslides and identified and described a strong correlation between sea-level rise and slope instability. Others (e.g., Posamentier and Vail, 1988; Christian et al., 1997; Talling et al., 2014) instead propose that

excess pore pressure could be generated during sea-level fall and lowstand, as documented in the western African margin (Rothwell et al., 1998), in the Central Adriatic basin (Trincardi et al., 2004), in the SW Iberian margin (Lebreiro et al., 1997), in the western Mediterranean (Rothwell et al., 2000), and in the south Adriatic margin (Minisini et al., 2006). Considering the aforementioned hypothesis and high similarity with the sequence stratigraphic model described in Posamentier and Vail (1988), we interpret sea-level fall as a trigger mechanism of TLC. Indeed, during sea-level fall and then during the last glacial interval (MIS2), when the sea level dropped to 120 m lower than today (Fairbanks, 1989; Siddal et al., 2003), the mapped MTD scars in our study area were characterised by lower hydrostatic pressure probably triggered during sea level fall (MTD1 and MTD2) and during lowstand (MTD3 and MTD4).

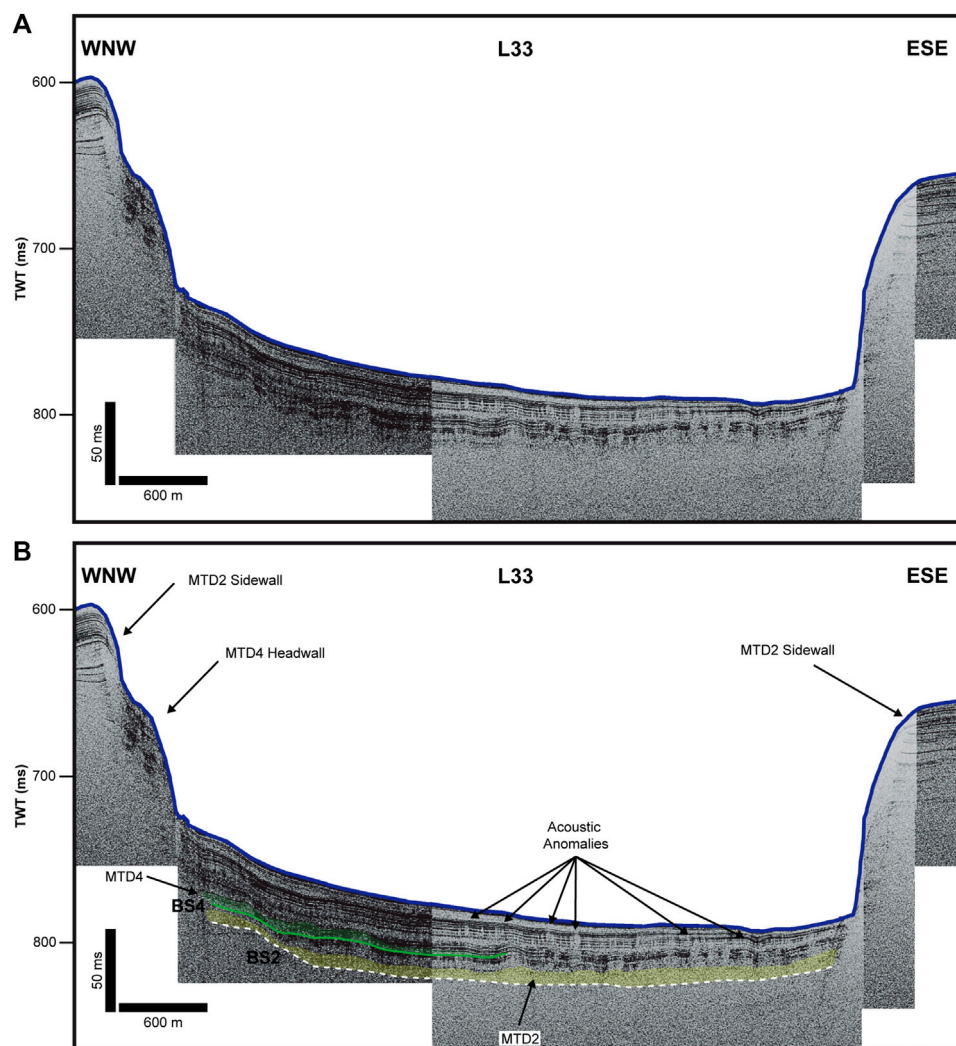


FIGURE 7

(A) Uninterpreted and (B) interpreted images of the CHIRP profile L33. The seismic profile shows the upper boundary of MTD4, which is characterized by the presence of the acoustic anomalies. The morphological features are also indicated (see Figure 1B for the location of the profile).

5.2.3 The role of weak layers

Weak layers are measured in decimetres or centimetres (L'Heureux et al., 2012; Sammartini et al., 2019; Gatter et al., 2020) and can be buried beneath metres of sediment, making identification very difficult (Gatter et al., 2021). However, Gatter et al. (2021) presented a classification of weak layers based on lithology. In particular, weak layers in siliciclastic sediments can form in softening sediments (clay layers). Clay layers may have poor or reduced shear strength. Although it is not possible to identify one or more layers from sediments sampled in a core (Meo et al., 2008b), it is possible to use the model proposed by Gatter et al. (2021) to define the identified muddy sediments as a probable weak layer in the TLC.

5.2.4 Free gas charge

In the TLC, several acoustic anomalies in the sediments have been identified on the sub-bottom CHIRP profiles. These features show no sub-bottom reflectors and subparallel divergent to

convergent reflectors. They were identified on the top of MTD4, making it difficult to define in some parts (Figures 3B, 7, 8A, B). We also identified them on top of MTD2, where they are present close to the seafloor (Figures 8C, D, 9). It is likely that the detected semi-transparent seismic facies can indicate the presence of gas chimneys. Indeed, some authors (Micallef et al., 2019; Spatola et al., 2020) associate similar seismic facies with the presence of gas in the sedimentary layers. Thus, the presence of gas above MTD2 and MTD4 may indicate a possible trigger mechanism for the more recent landslides, suggesting the possibility that it was a trigger for the whole TLC.

5.2.5 Tectonic factors

The evidence of multiple mass-transport deposits at several stratigraphic levels may have required a recurrent trigger (Minisini et al., 2007). In this case, seismicity is the most plausible trigger mechanism (e.g., Syvitski & Schafer, 1996; Schnellmann et al., 2002; Lamarche et al., 2008; Alves, 2015).

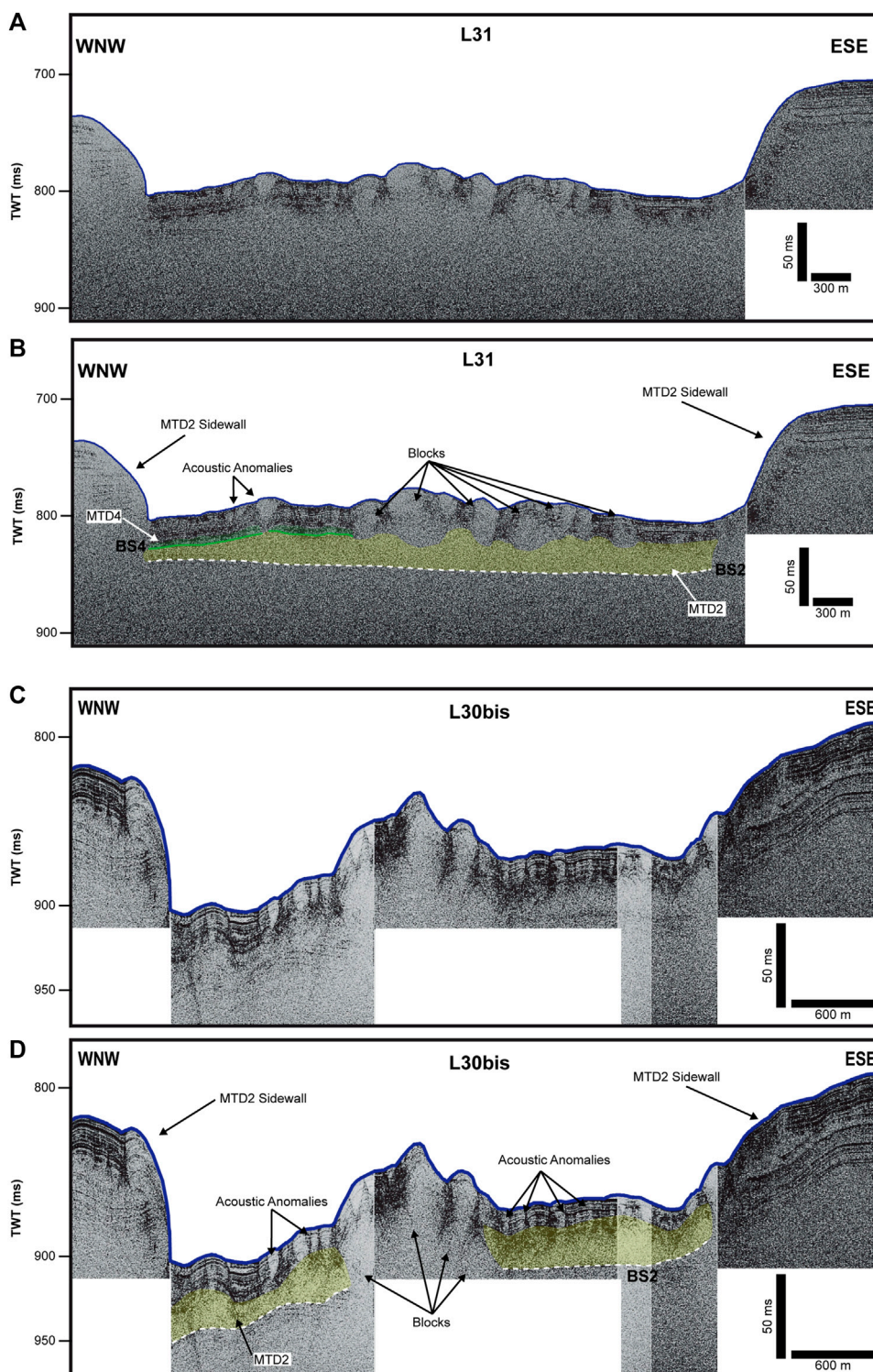


FIGURE 8

(A) Uninterpreted and (B) interpreted images of the CHIRP profile L31. The area is characterised by hummocky morphology, suggesting the presence of blocks in MTD2. Furthermore, acoustic anomalies are shown above the upper MTD4 boundary. (C) Uninterpreted and (D) interpreted images of the CHIRP profile L30bis. The profiles show only MTD2 with hummocky morphology and acoustic anomalies. The morphological features are also indicated (see Figure 1B for the location of the profile).

Several stages of tectonic activity have been identified in the Southern Apennines in the last 0.7 Ma BP (Ciaranfi et al., 1979; Patacca & Scandone, 1989; Patacca & Scandone, 2007).

The Gulf of Taranto is the southern Apennines accretionary wedge, and persistent upwards thrust activity to the latest Quaternary and possibly up to recent times has been

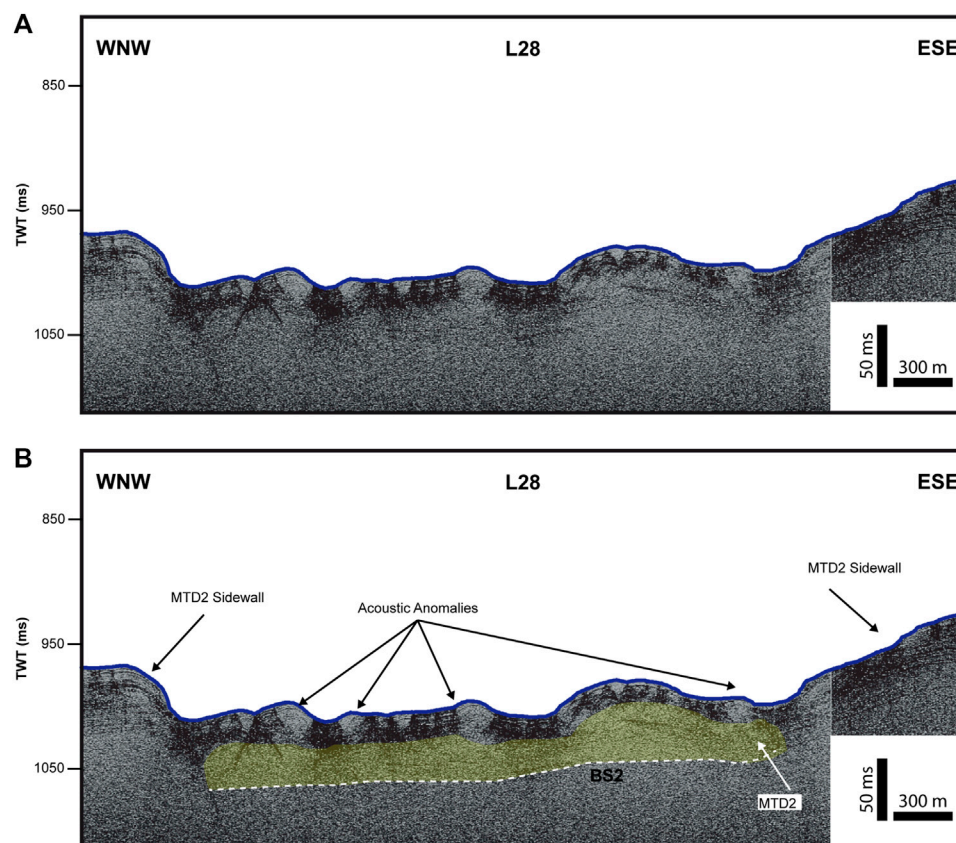


FIGURE 9
 (A) Uninterpreted and (B) interpreted images of the CHIRP profile L28. The hummocky morphology and acoustic anomalies are shown. The morphological features are also indicated (see Figure 1B for the location of the profile).

documented (Teofilo et al., 2018). According to Teofilo et al. (2018), the estimated slip-rate mean values on the deeper interplate surface are about 4 and 7 mm/y during the Messinian-Late Quaternary. In fact, they identified thrusts which could represent important seismogenic sources that can generate earthquakes of up to magnitudes of 6.8–7.3 (Wells and Coppersmith, 1994). Thus, the energy provided by earthquake shaking can represent a good trigger mechanism for submarine landslides on an open slope, with high gradients and under consolidated sediment conditions.

5.3 Comparison with some landslide complexes at the Mediterranean-global scale

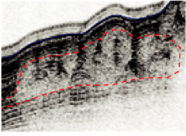
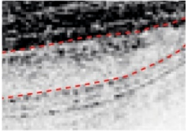
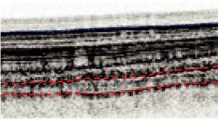
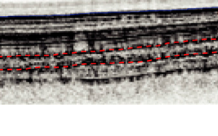
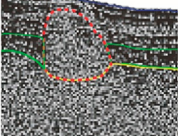
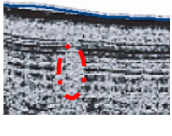
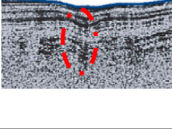
Recent acquisition of morphobathymetric data along the Apulian continental margin has allowed the mapping of several mass movements that allow us to define these as the most widespread sedimentary processes on the slope of this area (e.g., in the framework of MaGIC project, 2007–2012; Chiocci et al., 2021). Controversially, on the Apulian continental slope, the insights from this process have been very few (Ceramicola et al., 2012; Ceramicola et al., 2014), and the process is still poorly known. Comparing the TLC and other mass movements in the same area was thus not possible. Therefore, some important landslides at

the Mediterranean-global scale (in terms of mass movement types, shape, area, and estimated volume style of failures) were considered in order to better define the morphological features of the TLC and understand how the geological context influences the evolution of submarine landslides. There are five well-known landslide complexes: Storegga Slide, Afen Slide, Ana Slide, Chateleur-Mississippi, and BIG '95 (Bugge et al., 1988; Farràn and Maldonado, 1990; Graham et al., 1996; Masson et al., 1996; Canals et al., 2004; Hafidason et al., 2004; Lastras et al., 2004; Wilson et al., 2004; Micallef et al., 2008; Lafuerza et al., 2012; Martinez et al., 2022; Sager et al., 2022; Table 4).

One of the largest submarine landslides known is the Storegga Slide, located on the open slope of the passive Norwegian Margin (Canals et al., 2004). It was originally interpreted as consisting of three failure events, the first being the largest with a volume of 3,880 km³ (Bugge et al., 1988). Afterwards, Hafidason et al. (2004) identified several more individual failure events in the headwall region. TLC developed at the same depth of the Storegga Slide (200 m water depth) and the headwall region appears similar in morphology. Both show several flow phases while the TLC's area is much smaller, probably due to both the topography and thickness of sediment of the Apulian continental slope. Another difference concerns their development in space: Storegga has a retrogressive development while TLC shows a downslope development (Table 4).

Similar morphologies were identified with the Ana Slide, offshore of the Balearic Islands (Lastras et al., 2006; Berndt et al., 2012; Lafuerza

TABLE 3 Table showing identified acoustic facies in sub-bottom CHIRP profiles.

MTD name		Seismic facies	Relation to the underlying unit	
MTD1		From chaotic sub-bottom seismic reflectors to intermittent, indistinct, discontinuous sub-bottom with regular small hyperbolae	Moderate amplitude and continuity (bounding surface BS1)	3 and 4
MTD2		From chaotic sub-bottom seismic reflectors to intermittent, indistinct, discontinuous sub-bottom	Low-to-moderate amplitude and continuity (bounding surface BS2)	3, 5, 6, 7, 8, and 9
MTD3		From chaotic sub-bottom seismic reflectors to intermittent, indistinct, discontinuous sub-bottom with some small hyperbolae	Moderate amplitude and continuity (bounding surface BS3)	3, 5, and 9
MTD4		From chaotic sub-bottom seismic reflectors to intermittent, indistinct, discontinuous sub-bottom with some small hyperbolae	Low-to-moderate amplitude and continuity (bounding surface BS4)	3, 5, 6, 7, and 8
MTD5		From chaotic sub-bottom seismic reflectors to intermittent, indistinct, discontinuous sub-bottom	Moderate amplitude and continuity (bounding surface BS5)	3 and 5
BLOCK UNIT		Hummocky seafloor and no sub-bottom reflectors	Inside of MTD2 overlapped by MTD4	3 and 8
ACOUSTIC ANOMALIES (a)		No sub-bottom reflectors (free gas charge)		3, 7 and 9
ACOUSTIC ANOMALIES (b)		Subparallel divergent to convergent reflectors (free gas charge)		3, 7, and 8

et al., 2012; Sager et al., 2022). They both present a similar source area, almost completely evacuated with several small headscarps, and two well developed sidewalls. However, the shape of the Ana slide headwall shows a retrogressive development (Micallef et al., 2008) while the TLC evolves downslope. Furthermore, the Ana Slide’s volume (0.06 km³) is smaller than the TLC’s (0.47 km³). Moreover, the areal extension, runout, and depths of development also appear to be different (Table 4).

The Afen Slide (Graham et al., 1996; Masson et al., 1996) on the west Shetland Slope is very similar to the TLC. Indeed, the Afen Slide’s overall runout is about 12 km, and the maximum width is

about 4.5 km (Wilson et al., 2004) while the TLC runout is 10 km and its maximum width is about 4.0 km. Moreover, the Afen Slide seems to show at least four major phases of failure and the TLC shows five. The shape of both landslide complexes is very similar, with several small headscarps. The main difference between them concerns development: Afen develops from 825 m to 1,120 m and has a slope angle of 1,5° while TLC develops from 200 m to 800 m with a greater slope angle (Table 4).

The BIG ’95 landslide on the Ebro continental slope in the western Mediterranean appears completely different, so it is difficult

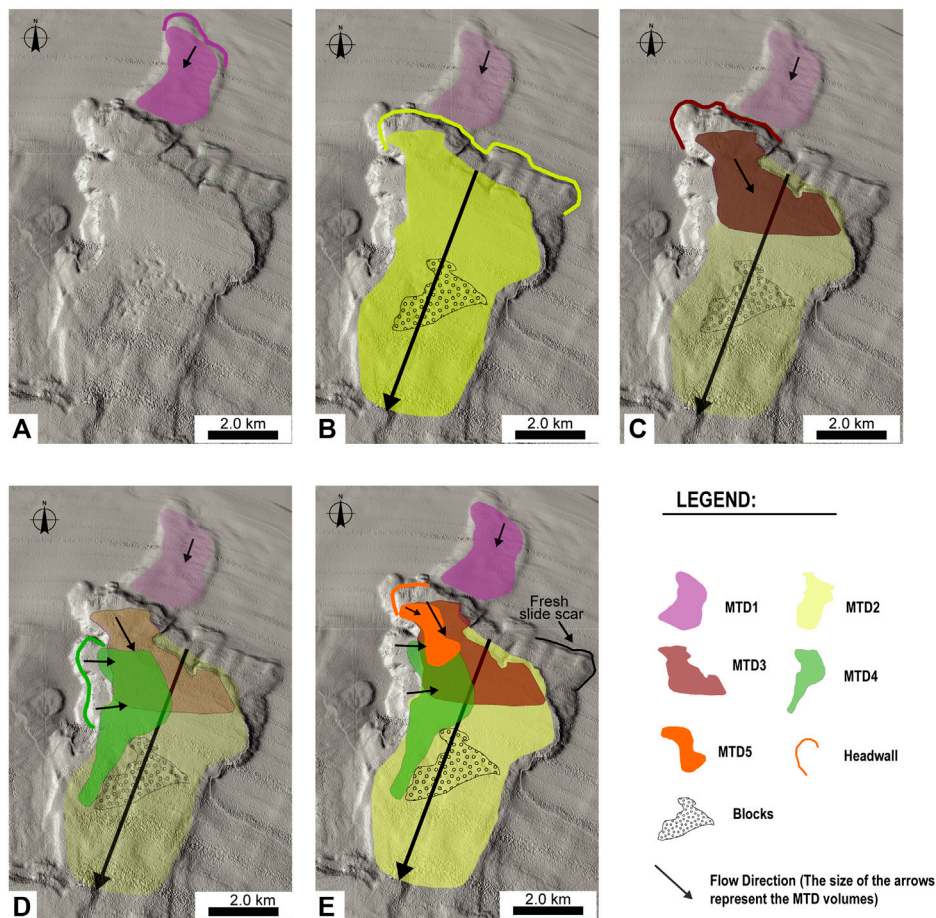


FIGURE 10
 Proposed scenario for relative slide timing based on the overlap and location of different mass transport deposits: (A) MTD1, (B) MTD2, (C) MTD3, (D) MTD4, and (E) MTD5. The arrows represent the flow direction. The size of the arrow represents the volume of each MTD. The line of the same colour as the deposit is the headwall.

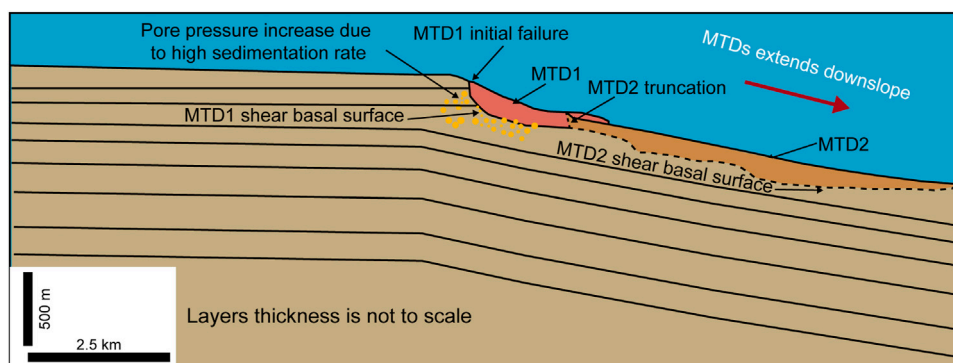


FIGURE 11
 Schematic model of the starting mechanisms of the submarine landslides. Landslide initiated from the upper slope due to rapid sedimentation (modified from Masson et al., 2008). Sediment thickness not to scale.

to compare with the TLC. Indeed, Canals et al. (2004) identified mass transport deposits covering about 2000 km² with a total volume of about 26 km³. This last is probably due to a volcanic supply coming from some volcanic edifices in nearby areas (Canals

et al., 2004). In addition, Farràn and Maldonado (1990) identified a lowstand sedimentary depocentre of the paleo Ebro River on the outermost shelf and upper slope adjacent to the Columbretes Islets. This could have provided significant volumes of sediment.

TABLE 4 Comparison between some parameters of the most important submarine landslides worldwide.

Instability	Total area (km ²)	Total water depth range (m)	Total height (m)	MTD water depth range (m)	Length × width (km)	Max/average thickness (m)	Deposit covered area (km ²)	Volume (km ³)	General shape of the deposit	Mean slope angle (°)	Mean source area angle (°)	Total runout distance (km)
Storegga	90,000	130/3,850	3,720	290/3,850	770 × 115	200/60	85,000	≤3,000	Fan-like coalescing debris lobe	1.5°	23°	700
Ana Slide	6	635/815	180	785/815	4 × 1.5	?/44	≈2	0.06	Lobate shape	≈2°	≈5°	≈3
Chandeleur-Mississippi fan	1,000	1,100–2,700	1,600	1,500/2,700	70	500/300	>1,000	300	Strongly elongated with lobes that diverge from the main flow pathway	2°	≈15°	40–70
Afen	40	825/1,120	295	1,005/1,120	12 × 4.5	20/10	20	0.2	Lobate shape	1.5°	22°	≈7°
TLC	40	200/800	600	230/800	10 × 4	36/12	34	0.47	Lobate shape	5°	≈15°	≈10
BIG '95	>2000	<600/2000	>1,400	650/2000	110 × <30	135/16	2000	26	Overall horsetail shape	2°	10°	110

The bold values highlight the Taranto Landslide Complex (TLC).

Likewise, the Chandeleur Submarine Landslide Complex on the upper Mississippi Fan of the Gulf of Mexico (Martinez et al., 2022) appears much larger than the TLC, as develops at 1,100 m water depth, with an area of 1,000 km² and a volume of about 300 km³. According to the cited authors, the origin of the Chandeleur Submarine Complex is a result of overpressuring caused by upward-migrating salt diapirs. These characteristics are completely different from those of the TLC.

As shown by this comparison, submarine landslides occur in a wide range of settings, including offshore volcanic islands (Moore et al., 1989; Masson et al., 2002; Le Friant et al., 2015), active and passive continental margins (Kvalstad et al., 2005; Moscardelli et al., 2006; Brothers et al., 2016), and even in mid-ocean ridges (Hunt and Jarvis, 2020). Submarine landslides can occur on slopes less than 1° (Prior and Suhayda, 1979; McAdoo et al., 2000b; Masson et al., 2002; Ten Brink U.S. et al., 2009; Urlaub et al., 2015; Scarselli, 2020). The failed sediment can evolve into different styles of deformation, processes, and deposits characteristics that have led to a number of descriptive terms such as creeps, slides, slumps, flows, and falls (Hampton et al., 1996; Posamentier and Martinsen, 2011; Sawyer et al., 2012). The TLC has similar characteristics to various landslides identified in different contexts. However, the style and processes of the TLC are uncertain, so the generic name “MTD” has been used (Gee et al., 2007).

5.4 MTD model of implementation

Based on analysis of high-resolution morphobathymetric data, the identification of multiple submarine MTDs on the TLC allows the reconstruction of the phase relationships among successive failures. The relative activity of the landslides is based on the morphology relationships of each MTD. Furthermore, seismic correlation based on CHIRP profiles shows that MTD1 and MTD2, the first mass transport event, were contemporaneous and reached an overall area of over than 30 km² with a maximum runout of 7.3 km. Furthermore, even following the age defined from the correlation with sedimentation rate of the area (Grauel, 2012), we can establish that MTD1 and MTD2 occurred simultaneously during the falling stage of sea level dated 24–25 ky cal. BP (Figures 10A, B).

Above MTD1 and MTD2, we observe regular sedimentation in the TLC area (Figure 7). According to the sedimentation rate defined by Grauel (2012), the time lapse between the deposition of MTD2 and MTD3 is about 4–5 ky.

During the relative lowstand of sea level (20 ky BP), marginal marine depocentres shifted towards the outer shelf (Posamentier et al., 1992) and overpressure was generated. Therefore, disequilibrium conditions and potential slope failures could have occurred. The trigger of MTD3 and MTD4 in the TLC may have been caused by this mechanism (Figures 10C, D).

The last mass event is represented by MTD5; it covers the seafloor and is spread in a narrow area. It probably occurred asynchronously, possibly resulting from slope readjustments governed by local factors (Figure 10E).

6 Conclusion

The Taranto Landslide Complex (TLC) is an example of a group of submarine landslides detected with very high-resolution

morphobathymetric data and sub-bottom CHIRP profiles. The results indicate the presence of five mass transport deposits (MTDs). They occurred essentially in two time intervals: the first from 25–26 ky BP during sea level fall and the second about 20–21 ky BP, during sea level lowstand. The rapid sedimentation during the sea level falls and lowstand stage directly at the shelf break and on the continental slope were probably the main conditioning factors for destabilizing the area. These hydrodynamic and sedimentary conditions produce changes of pore pressure within the sediments that could increase the generation of weak layers in the deposit's stratification, with the consequence of submarine collapses. Moreover, evidence of acoustic anomalies in the sediments, interpreted as free gas charge, could represent potential contributors to slope instability. The thrusts identified by several studies of the area testify that the compressive regime is still active and could represent a good trigger mechanism for submarine landslides on an open slope.

Data availability statement

The original contributions presented in the study are included in the article/supplementary material; further inquiries can be directed to the corresponding author.

Author contributions

AM and MS proposed the study and interpreted data; AM acquired and elaborated data, wrote the original draft, and edited the figures; MS proofread the manuscript. All authors contributed to the article and approved the submitted version.

References

- Alves, T. M. (2010). 3D Seismic examples of differential compaction in mass-transport deposits and their effect on post-failure strata. *Mar. Geol.* 271 (3–4), 212–224. doi:10.1016/j.margeo.2010.02.014
- Alves, T. M. (2015). Submarine slide blocks and associated soft-sediment deformation in deep-water basins: A review. *Mar. Petroleum Geol.* 67, 262–285. doi:10.1016/j.margeo.2015.05.010
- Berndt, C., Costa, S., Canals, M., Camerlenghi, A., de Mol, B., and Saunders, M. (2012). Repeated slope failure linked to fluid migration: The Ana submarine landslide complex, eivissa channel, western Mediterranean Sea. *Earth Planet. Sci. Lett.* 319, 65–74. doi:10.1016/j.epsl.2011.11.045
- Bordoni, P., and Valensise, G. (1999). Deformation of the 125 ka marine terrace in Italy: Tectonic implications. *Geol. Soc. Lond. Spec. Publ.* 146 (1), 71–110. doi:10.1144/gsl.sp.1999.146.01.05
- Brothers, D. S., Haeussler, P. J., Liberty, L., Finlayson, D., Geist, E., Labay, K., et al. (2016). A submarine landslide source for the devastating 1964 Chenega tsunami, southern Alaska. *Earth Planet. Sci. Lett.* 438, 112–121. doi:10.1016/j.epsl.2016.01.008
- Bugge, T., Belderson, R. H., and Kenyon, N. H. (1988). The storegga slide. *Philosophical Trans. R. Soc. Lond. Ser. A, Math. Phys. Sci.* 325 (1586), 357–388. doi:10.1098/rsta.1988.0055
- Bull, S., Cartwright, J., and Huuse, M. (2009). A review of kinematic indicators from mass-transport complexes using 3D seismic data. *Mar. Petroleum Geol.* 26 (7), 1132–1151. doi:10.1016/j.margeo.2008.09.011
- Canals, M., Lastras, G., Urgeles, R., Casamor, J. L., Mienert, J., Cattaneo, A., et al. (2004). Slope failure dynamics and impacts from seafloor and shallow sub-seafloor geophysical data: Case studies from the COSTA project. *Mar. Geol.* 213 (1–4), 9–72. doi:10.1016/j.margeo.2004.10.001
- Caputo, R., Bianca, M., and D'Onofrio, R. (2010). The ionian marine terraces of southern Italy: Insights for the quaternary geodynamic evolution of the area. *Tectonics* 29, TC4005. doi:10.1029/2009TC002625
- Caputo, R., and Bianca, M. (2005). Morphological evidence of late quaternary thrusting in the bradanico foredeep. *Rend. Soc. Geol. It* 1, 75–76.
- Carannante, G., Graziano, R., Ruberti, D., and Simone, L. (1997). *Upper Cretaceous temperate-type open shelves from northern (Sardinia) and southern (Apennines-Apulia) Mesozoic Tethyan margins*. Dordrecht, Netherlands: Springer.
- Carminati, E., Lustrino, M., and Doglioni, C. (2012). Geodynamic evolution of the central and Western mediterranean: Tectonics vs. igneous petrology constraints. *Tectonophysics* 579, 173–192. doi:10.1016/j.tecto.2012.01.026
- Casalbore, D., Clementucci, R., Bosman, A., Chiocci, F. L., Martorelli, E., and Ridente, D. (2020a). Widespread mass-wasting processes off NE sicily (Italy): Insights from morpho-bathymetric analysis. *Geol. Soc. Lond. Spec. Publ.* 500 (1), 393–403. doi:10.1144/SP500-2019-195
- Casalbore, D., Passeri, F., Tommasi, P., Verrucci, L., Bosman, A., Romagnoli, C., et al. (2020b). Small-scale slope instability on the submarine flanks of insular volcanoes: The case-study of the Sciara del Fuoco slope (Stromboli). *Int. J. Earth Sci.* 109, 2643–2658. doi:10.1007/s00531-020-01853-5
- Catalano, R., Doglioni, C., and Merlini, S. (2001). On the mesozoic Ionian basin. *Geophys. J. Int.* 144 (1), 49–64. doi:10.1046/j.0956-540x.2000.01287.x
- Catalano, S., Monaco, C., Tortorici, L., Paltrinieri, W., and Steel, N. (2004). Neogene-Quaternary tectonic evolution of the southern Apennines. *Tectonics* 23 (2). doi:10.1029/2003TC001512
- Ceramicola, S., Praeg, D., Coste, M., Forlin, E., Cova, A., Colizza, E., et al. (2014). "Submarine mass-movements along the slopes of the active Ionian continental margins and their consequences for marine geohazards (Mediterranean Sea)," in *Submarine*

Funding

This work was supported by MaGIC Project (Marine Geohazards along the Italian Coasts) funded by the Italian Civil Protection Department and FRA 2019 (Fund of University of Sannio, Benevento, Italy-Academic Research) of the MRS.

Acknowledgments

The authors acknowledge the Italian National Research Projects MaGIC (Marine Geological Hazard along the Italian Coast) funded by the Italian Civil Protection Department and the Scientific Coordinator of the Project, Francesco Latino Chiocci, of the Sapienza University of Rome. The authors thank all editors and reviewers for their helpful comments and suggestions.

Conflict of interest

The authors declare that the research was conducted in the absence of any commercial or financial relationships that could be construed as a potential conflict of interest.

Publisher's note

All claims expressed in this article are solely those of the authors and do not necessarily represent those of their affiliated organizations, or those of the publisher, the editors, and the reviewers. Any product that may be evaluated in this article, or claim that may be made by its manufacturer, is not guaranteed or endorsed by the publisher.

- mass movements and their consequences: 6th international symposium (Berlin, Germany: Springer International Publishing), 295–306. doi:10.1007/978-3-319-00972-8_26
- Ceramicola, S., Tinti, S., Praeg, D., Zaniboni, F., and Planinsek, P. (2012). "Potential tsunamigenic hazard associated to submarine mass movement along the Ionian continental margin (Mediterranean Sea)," in *EGU general assembly conference abstracts* (Munich, Germany: European Geosciences Union), 10808.
- Cheng, C., Jiang, T., Kuang, Z., Ren, J., Liang, J., Lai, H., et al. (2021). Seismic characteristics and distributions of Quaternary mass transport deposits in the Qiongdongnan Basin, northern South China Sea. *Mar. Petroleum Geol.* 129, 105118–118. doi:10.1016/j.marpetgeo.2021.105118
- Chiocci, F. L., Budillon, F., Ceramicola, S., Gamberi, F., and Orrù, P. (2021). *Atlante dei lineamenti di pericolosità geologica dei mari italiani – risultati del progetto MaGIC*. Roma: CNR edizioni.
- Chiocci, F. L., and Ridente, D. (2011). Regional-scale seafloor mapping and geohazard assessment. The experience from the Italian project MaGIC (Marine Geohazards along the Italian Coasts). *Mar. Geophys. Res.* 32 (1–2), 13–23. doi:10.1007/s11001-011-9120-6
- Christian, H. A., Woeller, D. J., Robertson, P. K., and Courtney, R. C. (1997). Site investigations to evaluate flow liquefaction slides at Sand Heads, Fraser River delta. *Can. Geotechnical J.* 34 (3), 384–397. doi:10.1139/97-004
- Ciaranfi, N., Maggiore, M., Pieri, P., Rapisardi, L., Ricchetti, G., and Walsh, N. (1979). Considerazioni sulla neotettonica della Fossa bradanica. *Progetto Final. Geodin. del CNR* 251, 73–95.
- Cosentino, D., Cipollari, P., Marsili, P., and Scrocca, D. (2010). Geology of the central Apennines: A regional review. *J. virtual Explor.* 36 (11), 1–37. doi:10.3809/jvirtex.2010.00223
- D'Argenio, B., Pescatore, T., and Scandone, P. (1973). *Schema geologico dell'Appennino meridionale (Campania e Lucania)*. Freiburg im Breisgau, Germany: Verlag nicht ermittelbar.
- Dalla Valle, G., Gamberi, F., Rocchini, P., Minisini, D., Errera, A., Baglioni, L., et al. (2013). 3D seismic geomorphology of mass transport complexes in a foredeep basin: Examples from the Pleistocene of the Central Adriatic Basin (Mediterranean Sea). *Sediment. Geol.* 294, 127–141. doi:10.1016/j.sedgeo.2013.05.012
- Davies, R. J., and Clark, I. R. (2006). Submarine slope failure primed and triggered by silica and its diagenesis. *Basin Res.* 18 (3), 339–350. doi:10.1111/j.1365-2117.2006.00297.x
- Di Bucci, D., Caputo, R., Mastronuzzi, G., Fracassi, U., Selli, G., and Sansò, P. (2011). Quantitative analysis of extensional joints in the southern Adriatic foreland (Italy), and the active tectonics of the Apulia region. *J. Geodyn.* 51 (2–3), 141–155. doi:10.1016/j.jog.2010.01.012
- Dugan, B., and Flemings, P. B. (2000). Overpressure and fluid flow in the New Jersey continental slope: Implications for slope failure and cold seeps. *Science* 289 (5477), 288–291. doi:10.1126/science.289.5477.288
- Dugan, B., and Sheahan, T. C. (2012). Offshore sediment overpressures of passive margins: Mechanisms, measurement, and models. *Rev. Geophys.* 50 (3). doi:10.1029/2011RG000379
- EMSC (2013). The European–Mediterranean seismological Centre. <http://www.emsc-csem.org/>.
- Fairbanks, R. G. (1989). A 17,000-year glacio-eustatic sea level record: Influence of glacial melting rates on the younger dryas event and deep-ocean circulation. *Nature* 342 (6250), 637–642. doi:10.1038/342637a0
- Farrán, M. L., and Maldonado, A. (1990). The Ebro continental shelf: Quaternary seismic stratigraphy and growth patterns. *Mar. Geol.* 95 (3–4), 289–312. doi:10.1016/0025-3227(90)90121-Y
- Ferranti, L., Antonioli, F., Mauz, B., Amorosi, A., Dai Pra, G., Mastronuzzi, G., et al. (2006). Markers of the last interglacial sea-level high stand along the coast of Italy: Tectonic implications. *Quat. Int.* 145, 30–54. doi:10.1016/j.quaint.2005.07.009
- Finetti, I. (2003). The CROP profiles across the Mediterranean Sea (CROP mare I and II) (2003). *Mem. Descr. Carta Geol. D'It.* 12, 171–184.
- Forsberg, C. F., Solheim, A., Kvalstad, T. J., Vaidya, R., and Mohanty, S. (2007). "Slope instability and mass transport deposits on the Godavari River Delta, east Indian margin from a regional geological perspective," in *Submarine mass movements and their consequences: 3 international symposium* (Cham, Netherlands: Springer), 19–27. doi:10.1007/978-1-4020-6512-5_3
- Gamberi, F., Rovere, M., and Marani, M. (2011). Mass-transport complex evolution in a tectonically active margin (Gioia Basin, Southeastern Tyrrhenian Sea). *Mar. Geol.* 279 (1–4), 98–110. doi:10.1016/j.marpetgeo.2010.10.015
- Gamboa, D., Alves, T., Cartwright, J., and Terrinha, P. (2010). MTD distribution on a 'passive' continental margin: The Espírito Santo Basin (SE Brazil) during the Palaeogene. *Mar. Petroleum Geol.* 27, 1311–1324. doi:10.1016/j.marpetgeo.2010.05.008
- Gamboa, D., and Alves, T. M. (2015). Three-dimensional fault meshes and multi-layer shear in mass-transport blocks: Implications for fluid flow on continental margins. *Tectonophysics* 647, 21–32. doi:10.1016/j.tecto.2015.02.007
- Gee, M. J. R., Uy, H. S., Warren, J., Morley, C. K., and Lambiasi, J. J. (2007). The Brunei slide: A giant submarine landslide on the north west borneo margin revealed by 3D seismic data. *Mar. Geol.* 246 (1), 9–23. doi:10.1016/j.marpetgeo.2007.07.009
- Georgiopolou, A., Krastel, S., Finch, N., Zehn, K., McCarron, S., Huvenne, V. A. I., et al. (2018). On the timing and nature of the multiple phases of slope instability on eastern Rockall Bank, Northeast Atlantic. *Geochem. Geophys. Geosystems* 20. doi:10.31223/osf.io/cywnw
- Graham, C., Holmes, R., Wild, J. B., and Tulloch, G. (1996). Charles Darwin cruise 101C–geological observations. British Geological Survey Technical Report WB/96 C. <https://nora.nerc.ac.uk/id/eprint/32281/RR99004.pdf>.
- Grauel, A. L. (2012). PhD diss. Zurich: ETH Zurich. <https://www.research-collection.ethz.ch/bitstream/handle/20.500.11850/153557/1/eth-5827-01.pdf>. Calibration of the clumped isotope thermometer on foraminifera and its application to high-resolution climate reconstruction of the past 2500yr in the Gulf of Taranto (Eastern Mediterranean Sea).
- Gross, F., Mountjoy, J. J., Crutchley, G. J., Böttner, C., Koch, S., Bialas, J., et al. (2018). Free gas distribution and basal shear zone development in a subaqueous landslide–Insight from 3D seismic imaging of the Tuaheni Landslide Complex, New Zealand. *Earth Planet. Sci. Lett.* 502, 231–243. doi:10.1016/j.epsl.2018.09.002
- Hafliðason, H., Sejrup, H. P., Nygård, A., Mienert, J., Bryn, P., Lien, R., et al. (2004). The storegga slide: Architecture, geometry and slide development. *Mar. Geol.* 213 (1–4), 201–234. doi:10.1016/j.marpetgeo.2004.10.007
- Hampton, M. A., Lee, H. J., and Locat, J. (1996). Submarine landslides. *Rev. Geophys.* 34, 33–59. doi:10.1029/95RG03287
- Horozal, S., Bahk, J. J., Urgeles, R., Kim, G. Y., Cukur, D., Kim, S. P., et al. (2017). Mapping gas hydrate and fluid flow indicators and modeling gas hydrate stability zone (GHSZ) in the Ulleung Basin, East (Japan) Sea: Potential linkage between the occurrence of mass failures and gas hydrate dissociation. *Mar. Petroleum Geol.* 80, 171–191. doi:10.1016/j.marpetgeo.2016.12.001
- Horváth, F., and D'Argenio, B. (1985). Subsidence history and tectonics of Western Adria margin. *Ac Geol. Hun* 28, 1–2.
- Huhn, K., Arroyo, M., Cattaneo, A., Clare, M. A., Gràcia, E., Harbitz, C. B., et al. (2019). Modern submarine landslide complexes: A short review. *Submar. Landslides Subaqueous mass Transp. deposits outcrops seismic profiles* 15, 181–200. doi:10.1002/9781119500513.ch12
- Hühnerbach, V., and Masson, D. G. (2004). Landslides in the north atlantic and its adjacent seas: An analysis of their morphology, setting and behaviour. *Mar. Geol.* 213 (1–4), 343–362. doi:10.1016/j.marpetgeo.2004.10.013
- Hunt, J. E., and Jarvis, I. (2020). The lifecycle of mid-ocean ridge seamounts and their prodigious flank collapses. *Earth Planet. Sci. Lett.* 530, 115867. doi:10.1016/j.epsl.2019.115867
- Iannace, A., Capuano, M., and Galluccio, L. (2011). Dolomites and dolomites in Mesozoic platform carbonates of the Southern Apennines: Geometric distribution, petrography and geochemistry. *Palaeogeogr. Palaeoclimatol. Palaeoecol.* 310 (3–4), 324–339. doi:10.1016/j.palaeo.2011.07.025
- ISIDe working Group (2016). Italian seismological instrumental and parametric database. <http://iside.rm.ingv.it/iside/standard/index.jsp>. doi:10.13127/ISIDeISIDe
- Kawamura, K., Laberg, J. S., and Kanamatsu, T. (2014). Potential tsunamigenic submarine landslides in active margins. *Mar. Geol.* 356, 44–49. doi:10.1016/j.marpetgeo.2014.03.007
- Kvalstad, T. J., Andresen, L., Forsberg, C. F., Berg, K., Bryn, P., and Wangen, M. (2005). The storegga slide: Evaluation of triggering sources and slide mechanics. *Mar. Petroleum Geol.* 22, 245–256. doi:10.1016/j.marpetgeo.2004.10.019
- Lamarche, G., Joanne, C., and Collot, J. Y. (2008). Successive, large mass-transport deposits in the south Kermadec fore-arc basin, New Zealand: The Matakaoa Submarine Instability Complex. *Geochem. Geophys. Geosystems* 9 (4). doi:10.1029/2007GC001843
- Lafuerza, S., Sultan, N., Canals, M., Lastras, G., Cattaneo, A., Frigola, J., et al. (2012). Failure mechanisms of Ana slide from geotechnical evidence, eivissa channel, western Mediterranean Sea. *Mar. Geol.* 307, 1–21. doi:10.1016/j.marpetgeo.2012.02.010
- Lastras, G., Canals, M., Amblas, D., Ivanov, M., Dennielou, B., Droz, L., et al. (2006). TTR-14 leg 3 shipboard scientific party eivissa slides, Western Mediterranean Sea: Morphology and processes. *Geo-Marine Lett.* 26, 225–233. doi:10.1007/s00367-006-0032-4
- Lastras, G., Canals, M., Hughes-Clarke, J. E., Moreno, A., Batist, M. D., Masson, D. G., et al. (2002). Seafloor imagery from the BIG'95 debris flow, Western Mediterranean. *Geology* 30, 871–874. doi:10.1130/0091-7613(2002)030<0871:sifbds>2.0.co;2
- Lastras, G., Canals, M., Urgeles, R., Hughes-Clarke, J. E., and Acosta, J. (2004). Shallow slides and pockmark swarms in the Eivissa Channel, Western Mediterranean Sea: Shallow slides and pockmark swarms. *Sedimentology* 51, 837–850. doi:10.1111/j.1365-3091.2004.00654.x
- Le Friant, A., Ishizuka, O., Boudon, G., Palmer, M. R., Talling, P. J., Villemant, B., et al. (2015). Submarine record of volcanic island construction and collapse in the Lesser Antilles arc: First scientific drilling of submarine volcanic island landslides by IODP Expedition 340. *Geochem. Geophys. Geosystems* 16 (2), 420–442. doi:10.1002/2014GC005652
- Lebreiro, S. M., McCave, I. N., and Weaver, P. P. (1997). Late Quaternary turbidite emplacement on the Horseshoe abyssal plain (Iberian margin). *J. Sediment. Res.* 67 (5), 856–870. doi:10.1306/D4268658-2B26-11D7-8648000102C1865D

- Lee, H. J. (2009). Timing of occurrence of large submarine landslides on the Atlantic Ocean margin. *Mar. Geol.* 264 (1-2), 53–64. doi:10.1016/j.margeo.2008.09.009
- Leynaud, D., Mienert, J., and Vanneste, M. (2009). Submarine mass movements on glaciated and non-glaciated European continental margins: A review of triggering mechanisms and preconditions to failure. *Mar. Petroleum Geol.* 26 (5), 618–632. doi:10.1016/j.marpetgeo.2008.02.008
- Locat, J., and Lee, H. J. (2002). Submarine landslides: Advances and challenges. *Can. Geotechnical J.* 39 (1), 193–212. doi:10.1139/t01-089
- Maslin, M., Vilela, C., Mikkelsen, N., and Grootes, P. (2005). Causes of catastrophic sediment failures of the Amazon Fan. *Quat. Sci. Rev.* 24 (20-21), 2180–2193. doi:10.1016/j.quascirev.2005.01.016
- Masson, D. G., Bett, B. J., and Birch, K. G. (1996). “Integrated environmental survey of 20,000 km² of seafloor west of Shetland: Preliminary results,” in *Towards 200 metres or millenium? Deepwater site investigation* (London UK).
- Masson, D. G., Harbitz, C. B., Wynn, R. B., Pedersen, G., and Lovholt, F. (2006). Submarine landslides: Processes, triggers and hazard prediction. *Philosophical Trans. R. Soc. A Math. Phys. Eng. Sci.* 364 (1845), 2009–2039. doi:10.1098/rsta.2006.1810
- Masson, D. G., Le Bas, T. P., Grevemeyer, I., and Weinrebe, W. (2008). Flank collapse and large-scale landsliding in the Cape Verde islands, off west africa. *Geochem. Geophys. Geosyst* 9 (7), 1–16. doi:10.1029/2008GC001983
- Masson, D. G., Watts, A. B., Gee, M. J. R., Urgeles, R., Mitchell, N. C., Le Bas, T. P., et al. (2002). Slope failures on the flanks of the Western canary islands. *Earth-Science Rev.* 57 (1-2), 1–35. doi:10.1016/S0012-8252(01)00069-1
- Mastroruzzi, G., Caputo, R., Di Bucci, D., Fracassi, U., Iurilli, V., Milella, M., et al. (2011). Middle-Late Pleistocene evolution of the adriatic coastline of southern Apulia (Italy) in: Response to relative sea-level changes. *Geogr. Fis. Din. Quat.* 34, 207–221. doi:10.4461/gfdq.2011.34.19
- Mazzoli, S., Barkham, S., Cello, G., Gambini, R., Mattioni, L., Shiner, P., et al. (2001). Reconstruction of continental margin architecture deformed by the contraction of the Lagonegro Basin, southern Apennines, Italy. *J. Geol. Soc.* 158 (2), 309–319. doi:10.1144/jgs.158.2.309
- McAdoo, B. G., Pratson, L. F., and Orange, D. L. (2000a). Submarine landslide geomorphology, US continental slope. *Mar. Geol.* 169 (1-2), 103–136. doi:10.1016/S0025-3227(00)00050-5
- McAdoo, B. G., Pratson, L. F., and Orange, D. L. (2000b). Submarine landslide geomorphology, US continental slope. *Mar. Geol.* 169 (1-2), 103–136. doi:10.1016/S0025-3227(00)00050-5
- Meo, A., Falco, M., Chiocci, F. L., and Senatore, M. R. (2018a). “Kinematics and the tsunamigenic potential of Taranto landslide (northeastern Ionian Sea): Morphological analysis and modeling,” in *Landslides and engineered slopes. Experience, theory and practice* (Boca Raton, FL, USA: CRC Press), 1409–1416.
- Meo, A., Falco, M., Ercilla, G., Alonso, B., and Senatore, M. R. (2018b). Sedimentological analyses to identify centennial-scale climatic variability during the upper holocene: A gravity core collected on the Apulia continental slope in the Gulf of Taranto, Proceedings of the 2018 IEEE International Workshop on Metrology for the Sea: Learning to Measure Sea Health Parameters (MetroSea), Bari, Italy, doi:10.1109/MetroSea.2018.8657826
- Merlini, S., and Mostardini, F. (1986). Appennino centro-meridionale: Sezioni geologiche e proposta di modello strutturale. *In* *Geologia dell'Italia Cent. Congr. Naz.* 73, 147–149.
- Micallef, A., Berndt, C., Masson, D. G., and Stow, D. A. (2008). Scale invariant characteristics of the Storegga Slide and implications for large-scale submarine mass movements. *Mar. Geol.* 247 (1-2), 46–60. doi:10.1016/j.margeo.2007.08.003
- Micallef, A., Spatola, D., Caracausi, A., Italiano, F., Barreca, G., D'Amico, S., et al. (2019). Active degassing across the Maltese islands (Mediterranean Sea) and implications for its neotectonics. *Mar. Petroleum Geol.* 104, 361–374. doi:10.1016/j.marpetgeo.2019.03.033
- Minisini, D., Trincardi, F., and Asioli, A. (2006). Evidence of slope instability in the southwestern adriatic margin. *Nat. Hazards Earth Syst. Sci.* 6 (1), 217–240. doi:10.1111/j.1365-2117.2007.00324.x
- Minisini, D., Trincardi, F., Asioli, A., Canu, M., and Fogliani, F. (2007). Morphologic variability of exposed mass-transport deposits on the eastern slope of Gela Basin (Sicily channel). *Basin Res.* 19 (2), 217–240. doi:10.1111/j.1365-2117.2007.00324
- Moore, J. G., Clague, D. A., Holcomb, R. T., Lipman, P. W., Normark, W. R., and Torresan, M. E. (1989). Prodigious submarine landslides on the Hawaiian Ridge. *J. Geophys. Res. Solid Earth* 94 (B12), 17465–17484. doi:10.1029/JB094iB12p17465
- Moscaredelli, L., Wood, L., and Mann, P. (2006). Mass-transport complexes and associated processes in the offshore area of Trinidad and Venezuela. *AAPG Bull.* 90 (7), 1059–1088. doi:10.1306/02210605052
- Moscaredelli, L., and Wood, L. (2008). New classification system for mass transport complexes in offshore Trinidad. *Basin Res.* 20 (1), 73–98. doi:10.1111/j.1365-2117.2007.00340.x
- Mulder, T., and Cochonot, P. (1996). Classification of offshore mass movements. *J. Sediment. Res.* 66, 43–57. doi:10.1306/D42682AC-2B26-11D7-8648000102C1865D
- Omeru, T., and Cartwright, J. A. (2015). Multistage, progressive slope failure in the Pleistocene pro-deltaic slope of the west Nile delta (eastern mediterranean). *Mar. Geol.* 362, 76–92. doi:10.1016/j.margeo.2015.01.012
- Owen, M., Day, S., and Maslin, M. (2007). Late Pleistocene submarine mass movements: Occurrence and causes. *Quat. Sci. Rev.* 26 (7-8), 958–978. doi:10.1016/j.quascirev.2006.12.011
- Patacca, E., and Scandone, P. (2007). Geological interpretation of the CROP-04 seismic line (Southern Apennines, Italy). *Boll. Soc. Geol. Ital.* 7, 297–315.
- Patacca, E., and Scandone, P. (1989). *Post-Tortonian mountain building in the Apennines. The role of the passive sinking of a relic lithosphere slab*. New York, NY, USA.
- Pescatore, T., and Senatore, M. R. (1986). A comparison between a present-day (Taranto Gulf) and a miocene (irpinian basin) foredeep of the southern Apennines (Italy). *Special Publ. Int. Assoc. Sedimentologists* 8, 169–182.
- Posamentier, H. W., Allen, G. P., James, D. P., and Tesson, M. (1992). Forced regressions in a sequence stratigraphic framework: Concepts, examples, and exploration significance. *AAPG Bull.* 76 (11), 1687–1709.
- Posamentier, H. W., and Martinsen, O. J. (2011). The character and Genesis of submarine mass-transport deposits. *insights outcrop 3D seismic data* 96. doi:10.2110/sepm09.06.007
- Posamentier, H. W., and Vail, P. R. (1988). “Eustatic control on clastic deposition, II- sequence and systems tract models,” in *sea-level changes – an integrated approach*. C. K. Wilgus, B. S. Hastings, C. G. S. C. Kendall, et al. (Germany: Soc. Economic Pale).
- Prior, D. B., and Suhayda, J. N. (1979). Application of infinite slope analysis to subaqueous sediment instability, Mississippi Delta. *Eng. Geol.* 14 (1), 1–10. doi:10.1016/0013-7952(79)90059-0
- Rothwell, R. G., Reeder, M. S., Anastasakis, G., Stow, D. A. V., Thomson, J., and Kähler, G. (2000). Low sea-level stand emplacement of megaturbidites in the Western and eastern Mediterranean Sea. *Sediment. Geol.* 135 (1-4), 75–88. doi:10.1016/S0037-0738(00)00064-6
- Rothwell, R. G., Thomson, J., and Kähler, G. (1998). Low-sea-level emplacement of a very large late Pleistocene ‘megaturbidite’ in the Western Mediterranean Sea. *Nature* 392 (6674), 377–380. doi:10.1038/32871
- Rovere, M., Gamberi, F., Mercorella, A., and Leidi, E. (2014). Geomorphometry of a submarine mass-transport complex and relationships with active faults in a rapidly uplifting margin (Gioia Basin, NE Sicily margin). *Mar. Geol.* 356, 31–43. doi:10.1016/j.margeo.2013.06.003
- Sager, T. F., Urlaub, M., Kaminski, P., Papenberg, C., Lastras, G., Canals, M., et al. (2022). Development and emplacement of Ana slide, evivisa channel, western Mediterranean Sea. *Geochem. Geophys. Geosystems* 23. doi:10.1029/2022GC010469
- Sammartini, M., Camerlenghi, A., Budillon, F., Insinga, D. D., Zgur, F., Conforti, A., et al. (2019). Open-slope, translational submarine landslide in a tectonically active volcanic continental margin (Licosa submarine landslide, southern Tyrrhenian Sea). *Geol. Soc. Lond. Spec. Publ.* 477 (1), 133–150. doi:10.1144/SP477.34
- Sawyer, D. E., Flemings, P. B., Mohrig, D., and Buttles, J. (2012). Mudflow transport behavior and deposit morphology: Role of shear stress to yield strength ratio in subaqueous experiments. *Mar. Geol.* 307–310, 28–39. doi:10.1016/j.margeo.2012.01.009
- Scarselli, N. (2020). “Submarine landslides—architecture, controlling factors and environments,” in *A summary InRegional geology and tectonics* (Amsterdam, Netherlands: Elsevier), 417–439. doi:10.1016/B978-0-444-64134-2.00015-8
- Schnellmann, M., Anselmetti, F. S., Giardini, D., McKenzie, J. A., and Ward, S. N. (2002). Prehistoric earthquake history revealed by lacustrine slump deposits. *Geology* 30 (12), 1131–1134. doi:10.1130/0091-7613(2002)030<1131:pehrbl>2.0.co;2
- Senatore, M. R. (1988). *Comparazione tra i depositi plio-pleistocenici del bacino di Gallipoli (golfo di Taranto) e la successione miocenica del flysch di Faeto (unità irpine, monti della Daunia): Confronto tra l'avanfossa attuale e quella miocenica dell'Appennino meridionale (italia)*. Napoli, Roma: Consorzio Univ. Napoli e Palermo, Sede consorziata Napoli.
- Senatore, M. R., Meo, A., and Budillon, F. (2022). “Measurements in marine geology: An example in the Gulf of Taranto (northern Ionian Sea),” in *Measurement for the sea: Supporting the marine environment and the blue economy* (Cham, Switzerland: Springer International Publishing), 271–289. doi:10.1007/978-3-030-82024-4_11
- Senatore, M. R., Meo, A., Bosman, A., Casalbore, D., Chiocci, F. L., and Lai, E., *Morelli E foglio 43 Taranto*, (2021b) Atlante dei lineamenti di pericolosità geologica dei mari italiani - risultati del progetto MaGIC. CNR edizioni, Roma.
- Senatore, M. R., Meo, A., Bosman, A., Chiocci, F. L., and Lai, E. (2021a). “Atlante dei lineamenti di pericolosità geologica dei mari italiani Risultati del progetto MaGIC,” in *Foglio 42 metaponto* (Roma: CNR edizioni).
- Senatore, M. R., Normark, W. R., Pescatore, T., and Rossi, S. (1988). Structural framework of the Gulf of Taranto (Ionian Sea). *Mem. della Soc. Geol. d'Italia* 41 (4), 533–539.
- Shanmugam, G., and Wang, Y. (2015). The landslide problem. *J. Palaeogeogr.* 4 (2), 109–166. doi:10.3724/SP.J.1261.2015.00071
- Siddall, M., Rohling, E. J., Almogi-Labin, A., Hemleben, C., Meischner, D., Schmelzer, I., et al. (2003). Sea-level fluctuations during the last glacial cycle. *Nature* 423 (6942), 853–858. doi:10.1038/nature01690
- Skarke, A., Ruppel, C., Kodis, M., Brothers, D., and Lobecker, E. (2014). Widespread methane leakage from the sea floor on the northern US Atlantic margin. *Nat. Geosci.* 7 (9), 657–661. doi:10.1038/NGEO2232

- Smith, D. E., Harrison, S., and Jordan, J. T. (2013). Sea level rise and submarine mass failures on open continental margins. *Quat. Sci. Rev.* 82, 93–103. doi:10.1016/j.quascirev.2013.10.012
- Spatola, D., del Moral-Erencia, J. D., Micallef, A., Camerlenghi, A., Garcia-Castellanos, D., Gupta, S., et al. (2020). A single-stage megaflood at the termination of the Messinian salinity crisis: Geophysical and modelling evidence from the eastern Mediterranean Basin. *Mar. Geol.* 430, 106337. doi:10.1016/j.margeo.2020.106337
- Spatola, D., Micallef, A., Sulli, A., Basilone, L., and Basilone, G. (2018b). Evidence of active fluid seepage (AFS) in the southern region of the central Mediterranean Sea. *Measurement* 128, 247–253. doi:10.1016/j.measurement.2018.06.058
- Spatola, D., Micallef, A., Sulli, A., Basilone, L., Ferreri, R., Basilone, G., et al. (2018a). The Graham bank (sicily channel, central Mediterranean Sea): Seafloor signatures of volcanic and tectonic controls. *Geomorphology* 318, 375–389. doi:10.1016/j.geomorph.2018.07.006
- Strasser, M., Moore, G. F., Kimura, G., Kopf, A. J., Underwood, M. B., Guo, J., et al. (2011). Slumping and mass transport deposition in the Nankai fore arc: Evidence from IODP drilling and 3-D reflection seismic data. *Geochem. Geophys. Geosystems* 12 (5). doi:10.1029/2010GC003431
- Sulli, A., Agate, M., Zizzo, E., Gasparo Morticelli, M., and Lo Iacono, C. (2021a). Geohazards of the san vito peninsula offshore (southwestern tyrrhenian sea). *J. Maps* 17 (3), 185–196. doi:10.1080/17445647.2020.1866703
- Sulli, A., Zizzo, E., Spatola, D., Morticelli, M. G., Agate, M., Iacono, C. L., et al. (2021b). Growth and geomorphic evolution of the Ustica volcanic complex at the Africa-Europe plate margin (Tyrrhenian Sea). *Geomorphology* 374, 107526. doi:10.1016/j.geomorph.2020.107526
- Sultan, N., Cochonat, P., Canals, M., Cattaneo, A., Dennielou, B., Hafidason, H., et al. (2004). Triggering mechanisms of slope instability processes and sediment failures on continental margins: A geotechnical approach. *Mar. Geol.* 213 (1-4), 291–321. doi:10.1016/j.margeo.2004.10.011
- Syvitski, J. P., and Schafer, C. T. (1996). Evidence for an earthquake-triggered basin collapse in Saguenay Fjord, Canada. *Sediment. Geol.* 104 (1-4), 127–153. doi:10.1016/0037-0738(95)00125-5
- Talling, P. J., Paull, C. K., and Piper, D. J. (2013). How are subaqueous sediment density flows triggered, what is their internal structure and how does it evolve? Direct observations from monitoring of active flows. *Earth-Science Rev.* 125, 244–287. doi:10.1016/j.earscirev.2013.07.005
- Talling, P. J., Clare, M. L., Urlaub, M., Pope, E., Hunt, J. E., and Watt, S. F. (2014). Large submarine landslides on continental slopes: Geohazards, methane release, and climate change. *Oceanography* 27 (2), 32–45. doi:10.5670/oceanog.2014.38
- Tappin, D. R., Watts, P., McMurtry, G. M., Lafoy, Y., and Matsumoto, T. (2001). The sissano, Papua New Guinea tsunami of July 1998—Offshore evidence on the source mechanism. *Mar. Geol.* 175 (1-4), 1–23. doi:10.1016/S0025-3227(01)00131-1
- Ten Brink, U. S., Lee, H. J., Geist, E. L., and Twichell, D. (2009). Assessment of tsunami hazard to the US East Coast using relationships between submarine landslides and earthquakes. *Mar. Geol.* 264 (1-2), 65–73. doi:10.1016/j.margeo.2008.05.011
- Teofilo, G., Antoncacci, I., and Caputo, R. (2018). Neogene-Quaternary evolution of the offshore sector of the Southern Apennines accretionary wedge, Gulf of Taranto, Italy. *Tectonophysics* 738, 16–32. doi:10.1016/j.tecto.2018.05.006
- Trincardi, F., Cattaneo, A., Correggiari, A., and Ridente, D. (2004). Evidence of soft sediment deformation, fluid escape, sediment failure and regional weak layers within the late Quaternary mud deposits of the Adriatic Sea. *Mar. Geol.* 213 (1-4), 91–119. doi:10.1016/j.margeo.2004.10.003
- Twichell, D. C., Chaytor, J. D., ten Brink, U. S., and Buczkowski, B. (2009). Morphology of late Quaternary submarine landslides along the U.S. Atlantic continental margin. *Mar. Geol.* 264, 4–15. doi:10.1016/j.margeo.2009.01.009
- Urgeles, R., and Camerlenghi, A. (2013). Submarine landslides of the Mediterranean Sea: Trigger mechanisms, dynamics, and frequency-magnitude distribution. *J. Geophys. Res. Earth Surf.* 118 (4), 2600–2618. doi:10.1002/2013JF002720
- Urlaub, M., Talling, P. J., and Masson, D. G. (2013). Timing and frequency of large submarine landslides: Implications for understanding triggers and future geohazard. *Quat. Sci. Rev.* 72, 63–82. doi:10.1016/j.quascirev.2013.04.020
- Urlaub, M., Talling, P. J., Zervos, A., and Masson, D. (2015). What causes large submarine landslides on low gradient (<2°) continental slopes with slow (~ 0.15 m/kyr) sediment accumulation? *J. Geophys. Res. Solid Earth* 120 (10), 6722–6739. doi:10.1002/2015JB012347
- Vitale, S., and Ciarcia, S. (2013). Tectono-stratigraphic and kinematic evolution of the southern Apennines/Calabria-Peloritani Terrane system (Italy). *Tectonophysics* 583, 164–182. doi:10.1016/j.tecto.2012.11.004
- Vitale, S., and Ciarcia, S. (2022). The dismembering of the adria platforms following the late cretaceous-eocene abortive rift: A review of the tectono-stratigraphic record in the southern Apennines. *Int. Geol. Rev.* 64 (20), 2866–2889. doi:10.1080/00206814.2021.2004559
- Vitale, S., Prinzi, E. P., Ciarcia, S., Sabbatino, M., Tramparulo, F. D. A., and Verazzo, G. (2019). Polyphase out-of-sequence thrusting and occurrence of marble detritus within the wedge-top basin deposits in the Mt. Massico (southern Apennines): Insights into the late Miocene tectonic evolution of the central Mediterranean. *Int. J. Earth Sci.* 108, 501–519. doi:10.1007/s00531-018-1664-0
- Wells, D. L., and Coppersmith, K. J. (1994). New empirical relationships among magnitude, rupture length, rupture width, rupture area, and surface displacement. *Bull. Seismol. Soc. Am.* 84 (4), 974–1002. doi:10.1785/BSSA0840040974
- Wilson, C. K., Long, D., and Bulat, J. (2004). The morphology, setting and processes of the Afen Slide. *Mar. Geol.* 213 (1-4), 149–167. doi:10.1016/j.margeo.2004.10.005
- Yamamoto, Y., Chiyonobu, S., Kanamatsu, T., Ahagon, N., Aoiike, K., Kamiya, N., et al. (2019). Repeated large-scale mass-transport deposits and consequent rapid sedimentation in the Western part of the Bay of Bengal, India. *Geol. Soc. Lond. Spec. Publ.* 477, 183–193. doi:10.1144/sp477.12